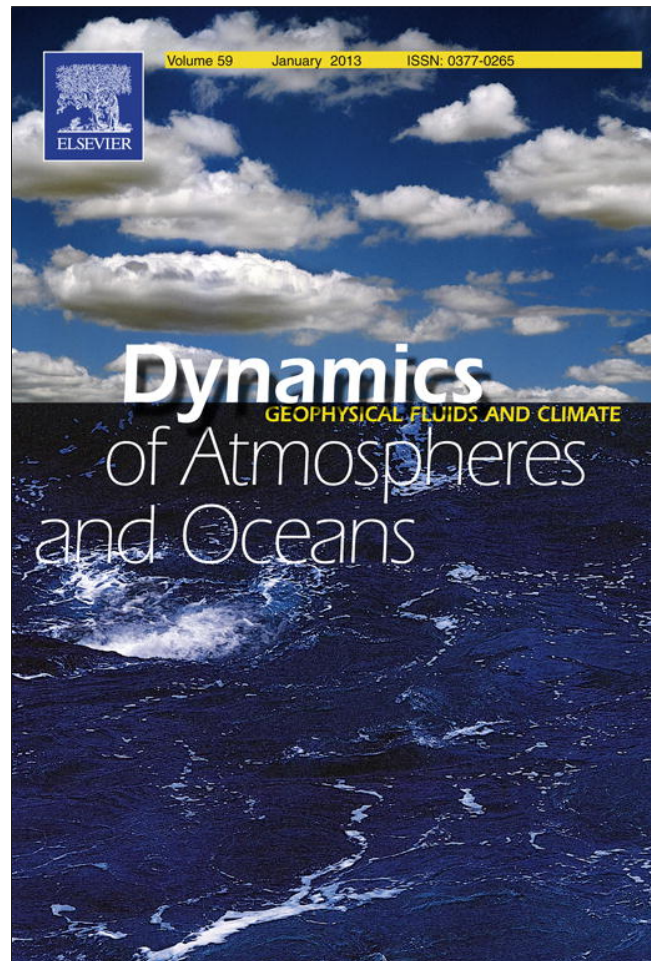


Provided for non-commercial research and education use.  
Not for reproduction, distribution or commercial use.



This article appeared in a journal published by Elsevier. The attached copy is furnished to the author for internal non-commercial research and education use, including for instruction at the authors institution and sharing with colleagues.

Other uses, including reproduction and distribution, or selling or licensing copies, or posting to personal, institutional or third party websites are prohibited.

In most cases authors are permitted to post their version of the article (e.g. in Word or Tex form) to their personal website or institutional repository. Authors requiring further information regarding Elsevier's archiving and manuscript policies are encouraged to visit:

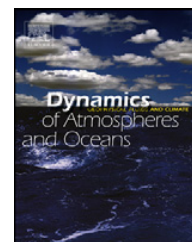
<http://www.elsevier.com/copyright>



Contents lists available at SciVerse ScienceDirect

## Dynamics of Atmospheres and Oceans

journal homepage: [www.elsevier.com/locate/dynatmoce](http://www.elsevier.com/locate/dynatmoce)



### Review

## Impact of interactive westerly wind bursts on CCSM3

Hosmay Lopez<sup>a,\*</sup>, Ben P. Kirtman<sup>a</sup>, Eli Tziperman<sup>b</sup>, Geoffrey Gebbie<sup>c</sup>

<sup>a</sup> Rosenstiel School of Marine and Atmospheric Science, Department of Meteorology and Physical Oceanography, University of Miami, Miami, FL, United States

<sup>b</sup> Department of Earth and Planetary Sciences, Harvard University, Cambridge, MA, United States

<sup>c</sup> Department of Physical Oceanography, Woods Hole Oceanographic Institution, Woods Hole, MA, United States

### ARTICLE INFO

#### Article history:

Received 17 November 2011

Received in revised form 18 October 2012

Accepted 28 November 2012

Available online 7 December 2012

#### Keywords:

Stochastic processes

Kelvin waves

Wind stress

ENSO

Coupled general circulation models

### ABSTRACT

Westerly wind bursts or events (WWBs or WWEs) are commonly viewed as stochastic processes, independent of any oceanic forcing. Some recent work and observations have suggested that these events can be viewed as state-dependent noise in that they are modulated by the SST variability. This potentially affects the predictability of the El Niño Southern Oscillation (ENSO). In this study, we examine the impact of parameterized WWBs on ENSO variability in the Community Climate System Model version 3.0 and 4.0 (CCSM3 and CCSM4). The WWBs parameterization is derived based on 50 years of atmospheric reanalysis data and observed estimates of tropical Pacific SST. To study the impact of WWBs three experiments are performed. In the first experiment, the model is integrated for several hundred years with no prescribed WWBs events (i.e. the control). In the second case, state-independent WWBs events are introduced. In other words, the occurrence, location, duration, and scale of the WWBs are determined (within bounds) randomly. These wind events are always positive (eastward) without a westward counterpart and are totally independent of the anomalies in the state variables, and can be thought of as additive noise. For the third case, the WWBs are introduced but as multiplicative noise or state-dependent forcing, modulated by SST anomalies.

The statistical moments for the Niño 3.4 index shows that the state-dependent case produced larger El Niño Southern Oscillation (ENSO) events and the bias toward stronger cold events is reduced as compared to the control and the state-independent runs. There is very little difference between the control and the state-independent WWB simulations suggesting that the deterministic

\* Corresponding author at: RSMAS/MPO, University of Miami, 4600 Rickenbacker Causeway, Miami, FL 33149, United States. Tel.: +1 305 298 8006.

E-mail address: [hlopez@rsmas.miami.edu](mailto:hlopez@rsmas.miami.edu) (H. Lopez).

component of the burst is responsible for reshaping the ENSO events. Lag-lead correlation of ocean variables with Niño 3.4 index suggests larger temporal coherence of the ENSO events. This, along with SSTA composites, also suggest a shift toward a more self-sustained mechanism as the experiments progress from the control to the state dependent WWBs. Overall, the parameterized WWBs have the capability to modify the ENSO regime in the CGCM, demonstrating the importance of sub-seasonal variability on interannual time scales. The fast varying (stochastic) component of WWB is of little importance, whereas the slow (SST dependent) component has a significant impact overall. The results are consistent between CCSM3 and CCSM4.

© 2012 Elsevier B.V. All rights reserved.

---

## Contents

1. Introduction .....	25
2. The couple model .....	27
3. Experiment description .....	28
3.1. State-dependent WWB parameterization .....	30
4. Observed versus parameterized WWBs .....	31
5. Results .....	33
6. Model sensitivity .....	43
7. Summary and discussion .....	47
Acknowledgments .....	49
References .....	49

---

## 1. Introduction

There are currently two main hypothesis that describe the lost of predictability of the tropical Pacific coupled system. One school of thought asserts that El Niño Southern Oscillation (ENSO) is intrinsically chaotic because of the nonlinear dynamics of the coupled system (Zebiak and Cane, 1987; Münnich et al., 1991; Jin et al., 1994; Tziperman et al., 1994, 1995; Chang et al., 1994; Zebiak, 1989; Wang et al., 1999), and while stochastic forcing can affect predictability, it is of secondary importance compared to the uncertainty in the initial conditions. Here, the slow component of the coupled system has two major natural modes of variability: the annual cycle, which is a response to external forcing, and internal modes (e.g. ENSO), which is due to air–sea coupling. ENSO interaction with the annual cycle could possibly produce irregularities and the loss of predictability. The second school of thought argues that the irregularity of ENSO and ultimately the loss of predictability are largely driven by stochastic forcing (e.g. Kirtman and Schopf, 1998; Eckert and Latif, 1997; Blanke et al., 1997; Penland and Matrosova, 1994; Penland and Sardeshmukh, 1995; Flügel and Chang, 1996; Moore and Kleeman, 1996; Kleeman and Moore, 1997; Xue et al., 1997; Chen et al., 1997; Moore and Kleeman, 1999a, b; Thompson and Battisti, 2001; Kleeman et al., 2003; Flügel et al., 2004; Zavala-Garay et al., 2003, 2004, 2005, 2008). If the stochastic forcing or noise is of primary importance then it is possible that the details (e.g. space–time structure and state dependence) of the noise are also important. McPhaden (2004) found that in order to predict ENSO development, it is not sufficient to know its preferable condition, (e.g. heat content buildup along the equator) highlighting the potential importance of stochastic forcing on the coupled system.

Implicitly stochastic view makes use of scale-separation to divide the tropical dynamic system into fast and slow time scales, although noise does occur on all space and time scales. Here, the fast time scale is originated from the life cycle of tropical atmospheric convection, while the slow time scale derives from the relaxation time of the ocean basin modified by air–sea coupling. If variability from the fast component projects onto the pattern of susceptibility, it could perturb the couple system.

These patterns may vary among different coupled models and the system may rapidly develop a very characteristic response, which in some coupled models strongly resembles a westerly wind burst (WWBs; Kleeman, 2008).

WWBs are an example of stochastic forcing of ENSO as they appear to be associated with internal variability of the atmosphere (e.g. Zhang and Gottschalck, 2002; Hendon et al., 2007) yet also seem to influence ENSO events. For example, Moore and Kleeman (1999a, b) calculated the stochastic optimal of an intermediate coupled model and argued that their spatial structure is consistent with the spatial structure associated with observed WWBs. In addition, Luther et al. (1983) concluded that the weakening of trade winds over the central Pacific before El Niño, from 1950 to 1978, was related to a series of strong WWBs. Westerly wind anomalies excite downwelling Kelvin waves that propagates eastward about the equator (Harrison and Schopf, 1984; McPhaden et al., 1988, 1992; McPhaden, 1999; Lengaigne et al., 2002). The effect of WWBs on sea surface temperature (SST) in the Pacific was studied by Vecchi and Harrison (2000). In this study, they found that WWBs represent a fundamental process for waveguide warming during the onset of El Niño and for eastern and central Pacific warm SSTA maintenance during El Niño.

These WWBs seem to result from various mechanisms, first from the Madden-Julian oscillation (MJO; Chen et al., 1996), however, a statistical relationship between the MJO and WWBs has not been well established. Zhang and Gottschalck (2002) indicated a tendency for larger SST anomalies of ENSO warm events in the eastern Pacific, to be preceded by stronger oceanic Kelvin wave anomalies induced by the MJO in the western Pacific. Second, cold surges from mid-latitude over the western Pacific (Love, 1985; Chu, 1988; Kiladis et al., 1994). Yu and Rienecker (1998) indicated in their case study of the 1997–98 El Niño that WWBs were associated with cyclones induced by a northerly surge in phase with the convective passage of the MJO. Yu et al. (2003) showed that changes in northerly surge pathways, influenced by ENSO phases, were related to WWB occurrences through cyclone formations over the western Pacific. However, it remains statistically unclear whether the surges are essential for WWB occurrences and the possibility that the MJO prepares the favorable environment for intrusion of cold surges. Third, WWBs can result from tropical cyclones (Keen, 1982), or a combination of the three (Yu and Rienecker, 1998). WWBs associated with twin cyclones over the western Pacific, accelerated the development of the 1986–87 El Niño event (Nitta and Motoki, 1987; Nitta, 1989). Murakami and Sumathipala (1989) emphasized that collective occurrences of WWBs lasting 7–20 days over the western Pacific were related to ENSO.

WWBs anomalies have amplitude of about  $7 \text{ m s}^{-1}$  and they may last for up to 20 days (Harrison and Vecchi, 1997). There is a large range of definitions for WWBs in the literature. Verbickas (1998) found that these bursts occur on average 3 times per year, with a higher incidence during the warm phase of ENSO (or El Niño). WWBs events are commonly viewed as completely stochastic processes, independent of any oceanic forcing. This is due to its short time scale, which may suggest they are external to equatorial Pacific interannual variability, although as recent literature suggests and as we argue here this is the subject of some debate.

Kirtman et al. (2005) used the so-called interactive ensemble coupling technique (Kirtman and Shukla, 2002; Kirtman et al., 2009) and found that the spatial structure of the dominant wind stress noise was remarkably similar to the spatial structure of the coupled signal and that the noise was state dependent. Moreover, Jin et al. (2007) formulated a simple coupled model to examine how state independent noise (i.e. additive) versus state dependent noise (i.e. multiplicative) affected ENSO variability. In that study, they found that unlike for additive noise, when the noise is state-dependent, it alters the ensemble mean evolution of ENSO, and also amplifies the ensemble spread during ensemble forecast. As the authors suggested, such findings challenge the view of ENSO as being a stable oscillator driven by additive noise.

Recent work has suggested that WWBs also contain a deterministic component, modulated by the SST. Based on observations, Yu et al. (2003) suggested that when the tropical Pacific warm pool is extended WWBs are more likely to occur. Tziperman and Yu (2007) analyzed scatterometer observations and showed that the characteristics of WWBs depend on the large-scale SST field and are therefore not purely stochastic. The 1997–98 El Niño, which was poorly predicted by most models, had a high occurrence of these wind bursts. During this ENSO event, WWBs were observed to migrate eastward with the  $29^\circ\text{C}$  SST isotherm (McPhaden, 1999). The western Pacific WWBs precede El Niño,

when the Pacific warm pool extends further east, and are not considered as purely stochastic (e.g. Zhang and Gottschalck, 2002; McPhaden et al., 2006; Seiki and Takayabu, 2007; Kug et al., 2008). WWBs induced by westerly background states associated with ENSO were shown using observational data (Seiki and Takayabu, 2007), GCM data (Kug et al., 2009; Sooraj et al., 2009), and CMIP3 multimodel data (Seiki et al., 2011). Seiki and Takayabu (2007) found that WWB frequencies for a western Pacific region were lag correlated with SST anomaly over the Niño-3 region. The same study hence found that WWBs tended to occur in sequence, from the western to eastern Pacific, leading the El Niño peak by 1–9 months.

Using a hybrid coupled model, Eisenman et al. (2005) showed that when the WWBs are dependent on SST, they have the same effect as strengthening ocean–atmosphere coupling. They also showed that when WWBs are fully deterministic, the ENSO events have twice the amplitude of that when the bursts are completely stochastic. This is due to the enhancement of the slow component (i.e. interannual component) of the WWBs (Roulston and Neelin, 2000). This potentially affects the ENSO predictability and prediction, because a stronger coupling can lead to a more self-sustained ENSO.

Here we advance a procedure for examining how both state dependent and state independent stochastic forcing affects ENSO variability in a sophisticated coupled model. While our focus is on state dependence, the approach can also be used to examine some elements of the sensitivity to the spatial structure. There are two aspects to our approach that we highlight here. First, we examine the impact of the stochastic forcing within the context of a state-of-the-art coupled general circulation model. Second, in terms of introducing the stochastic forcing, we take a phenomenological approach in that we focus on WWBs and parameterize their effect (both state independent and state dependent) in the coupled model. This is the first time that a state dependent and state independent WWB parameterization has been incorporated into a state-of-the-art coupled general circulation model.

The rest of this paper is organized as follows: Section 2 provides a discussion on the coupled models used. Section 3 describes the experimental design, including a short description of the WWBs parameterization. Section 4 compares some observed versus parameterized WWBs characteristics. Section 5 describes the results obtained from CCSM3 with parameterized WWBs and a comparison with a control run is made. Section 6 discusses the sensitivity of the results presented in 5 by implementing WWBs in CCSM4. Section 7 provides a summary and discussion of the results.

## 2. The couple model

The CGCM used in this work is the Community Climate System Model version 3 (CCSM3) and version 4 (CCSM4) from the National Center for Atmosphere Research (NCAR). This model is an earth system model comprised of four geophysical components consisting of atmosphere, land, ocean, and sea ice components all linked by a flux coupler. The coupler exchanges information among the components interactively while the model is running. The atmosphere is modeled by the Community Atmosphere Model (CAM). The land surface is modeled by the Community Land Surface Model (CLM). The oceans are represented using the Parallel Ocean Program (POP) and the sea ice is modeled by the Community Sea Ice (CSIM). Our work with the parameterized WWBs began using CCSM3, and as such most of the results are presented with this version of the coupled model. However, CCSM4 has become available and we have evaluated some of key results using this updated version of the coupled model.

For CCSM3 the atmosphere and land component models have horizontal resolution of T42 (128 longitude and 64 latitude points, or  $\sim 280$  km) and 26 vertical levels. For the POP and CSIM, the horizontal resolution is approximately  $1^\circ$  in the longitude and variable in the latitude direction with finer resolution, about  $1/3^\circ$ , near the equator. The POP has 40 vertical levels with level thickness monotonically increasing from approximately 10–250 m.

CCSM3 is a well-studied model with well-documented errors in its ENSO statistics (e.g. Collins et al., 2006). For example, SST anomalies associated with ENSO extend too far west in CCSM3 as compared to observations. This is consistent with the well-documented westward displacement of the mean eastern Pacific cold tongue position. Also, such SST anomalies show a strong meridional confinement about the equator as compared to observations. This confinement can be the result of significantly

narrow zonal wind stress forcing in CCSM3. Deser et al. (2006) found that the meridional confinement of zonal wind stress is indeed related to the high frequency of interannual variability in CCSM3 and is related to equatorial wave-guide ocean dynamics (see Kirtman, 1997). It is difficult to determine the dynamical regime of CCSM3. However, results from Kirtman et al. (2009) suggest that CCSM3 does not behave, as one would expect from a damped linear system. Non-linearity and coupled feedbacks are likely to be important.

Despite the well-known errors in ENSO statistics, CCSM3 has also been shown to have reasonable ENSO prediction skill. For instance, Kirtman and Min (2009) compared CCSM3 ENSO predictions to the operational NOAA Climate Forecasting System (CFS), and found that the both the deterministic and probabilistic forecast quality in the Niño3.4 region was comparable. Clearly the fidelity of ENSO in CCSM3 is arguable. As such, we have also tested the WWB parameterization implemented here in CCSM4. The experiments shown with CCSM4 primarily serve to suggest that the key results with the WWB parameterization are largely insensitive to substantial changes in the ENSO physics. Results using CCSM4 are described in Section 6.

There are significant improvements physically and numerically from CCSM3 to CCSM4, only some of those related to this study are noted here. The atmosphere component employs an improved deep convection scheme by inclusion of sub-grid convective momentum transport and a more realistic dilution approximation for the calculation of convective available potential energy (Neale et al., 2008). The atmospheric component of CCSM4 has the same 26 vertical levels, but with reduced horizontal resolution (i.e.  $5^\circ$  longitude by  $4^\circ$  latitude resolution). The dynamical core uses the finite volume formulation as opposed to the spectral dynamic core in CCSM3.

The ocean model component of CCSM4 uses Parallel Ocean Program version 2 (POP2) numerics (Danabasoglu et al., 2012). This updated version of POP includes a simplified version of the near boundary eddy flux parameterization of Ferrari et al. (2008), vertically-varying isopycnal diffusivity coefficients (Danabasoglu and Marshall, 2007), an abyssal tidally driven mixing parameterization, modified anisotropic horizontal viscosity coefficients with much lower magnitudes than in CCSM3 (Jochum et al., 2008), and a modified K-profile parameterization with horizontally varying background vertical diffusivity and viscosity coefficients (Jochum, 2009). The number of vertical levels has been increased from 40 levels in CCSM3 to 60 levels in CCSM4. The horizontal grid used here is a displaced pole version, with about  $3^\circ$  in the longitude and variable in the latitude direction with finer resolution, about  $1^\circ$ , near the equator.

Before describing the characteristics of the WWBs being added as noise in the model, it is important to note the general structure of the noise produced by the atmospheric component itself. By making use of the Interactive Ensemble technique (Kirtman et al., 2009), the atmospheric internal variability (noise) was separated from the signal for the zonal wind (not shown). Most of the noise activity occurs outside the observed WWB domain, and is largest in amplitude further east (from 160W to 120W). In fact, the noise is the strongest over the same region as the ensemble mean and it has greater amplitude during the cold phase of ENSO. But overall, its magnitude ( $U < +5 \text{ m s}^{-1}$ ) is under the lower bound of what would be considered the typically amplitude of a WWB ( $U > +5 \text{ m s}^{-1}$ ). This is one of the motivations for this work, the absence of observed features (WWB) in this model and its importance for ENSO. These winds do not match the observed temporal and spatial characteristics of WWBs. Given this, we have assumed that there is little or none WWBs activity in CCSM3, at least for the resolution used in these experiments.

### 3. Experiment description

Before describing the experiment setup, the authors would like to comment on the model used. Even though CCSM3 is known to have significant bias, it is considered a state-of-the-art climate system, and is still used in many studies (i.e. CMIP3 comparisons of ENSO – see DiNezio et al., 2012). The atmospheric component produces its own noise, which presumably occurs on all space and time scales. The Eisenman et al. (2005) results may be easier to interpret, but this is due to the simplicity of the model. It is unclear whether the Eisenman et al. (2005) can be generalized or understood within the context of a complex coupled model that attempts to simulate all the relevant physical and dynamical interactions associated with climate variability in the tropics. We do not argue that our results are

an “improvement” beyond Eisenman et al. (2005), but we do assert that attempting this problem in a sophisticated coupled CGCM is a natural follow on from this earlier work and does provide new insights.

The WWB parameterization is derived based on 50 years of atmospheric reanalysis data and observed estimates of tropical Pacific SST. The details of the parameterization are given in Gebbie and Tziperman (2009) and are followed without modification here. To study the impact of WWBs three experiments are performed. In the first experiment, the model (CCSM3) is integrated for several hundred years with no prescribed WWB events (i.e. control). In the second case, fully stochastic WWB events are introduced. In other words, the occurrence, location, duration, and scale of the WWBs are determined (within bounds) randomly. These wind events are always positive (eastward) without a westward counterpart and are totally independent of the state variables (e.g. SST), and can be thought of as additive noise.

For the purely stochastic case, the wind events associated with the WWBs are only dependent on the seasonal cycle. This is because the bursts are introduced in the model as noise with stationary statistics (e.g. Eckert and Latif, 1997). Given that the noise is stationary in time or only dependent on the seasonal cycle; its occurrence will not depend on interannual variability such as ENSO. The burst amplitude, position, fetch, and duration are random within some specified bounds.

For the third case, the WWB is introduced as multiplicative noise or state-dependent forcing, modulated by the SST. In this case, all aspects of the parameterized WWBs including the amplitude, scale, location, duration and probability of occurrence are dependent on the SSTA (see next sub-section for additional discussion of this dependence). An example of the parameterized WWBs is shown in Fig. 1. Here we show the parameterized zonal wind anomaly using observed estimates of the SSTA (Fig. 1; right panel), so in this case we are applying the state dependent formulation. Fig. 1 includes three

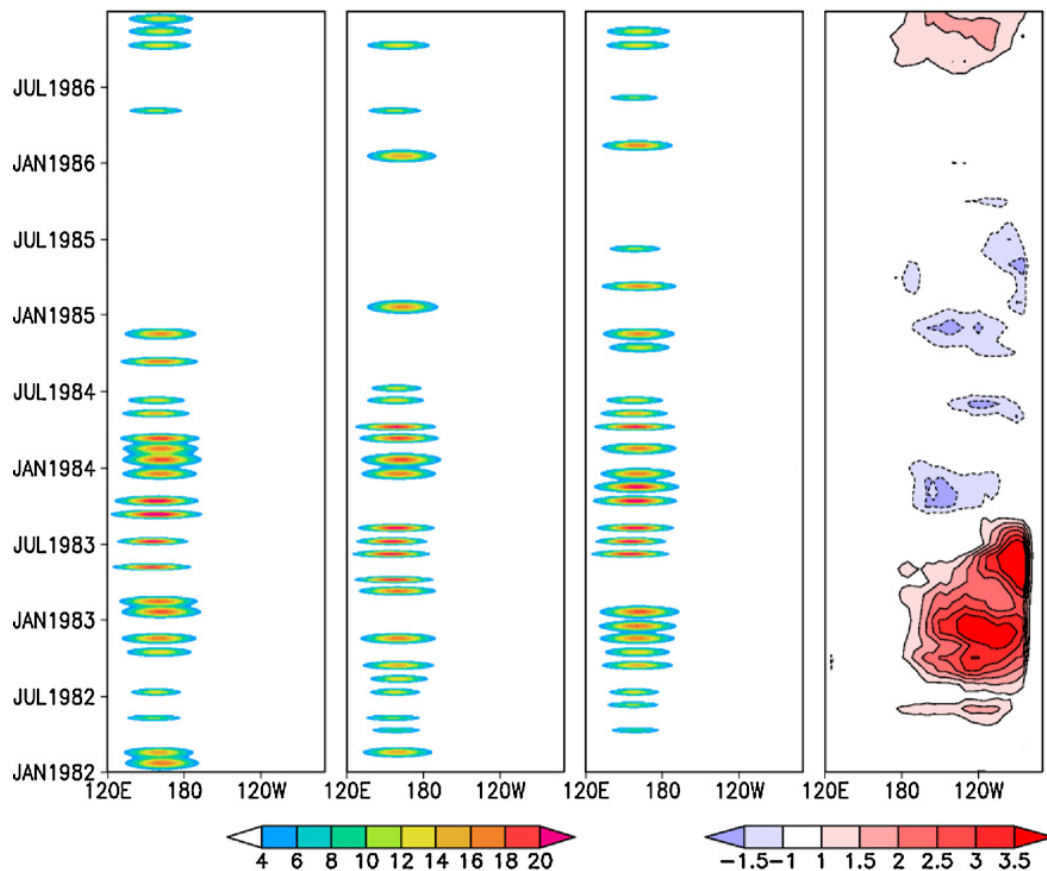


**Fig. 1.** Hovmöller diagram showing three state-dependent WWBs realizations (3 left panels) [ $\text{m s}^{-1}$ ] using the same observed SSTA (right panel) [ $^{\circ}\text{C}$ ], showing cross-section along the equatorial Pacific Ocean. Time increases up the page and covers from January 1982 to December 1986. Stochastic component depicted by the difference among the three realizations. The deterministic component is highlighted by the increased WWBs activity during warm events.

panels on the left each of which corresponds to a different realization of the parameterization, but with the same prescribed SSTA (right most panel). Differences among the three left panels indicate the stochastic component parameterization, but the preference for enhanced WWB activity during warm periods (i.e. the deterministic component) remain detectable in all three realizations. Fig. 1 demonstrates several properties of the parameterization. For example, the duration, the amplitude, the location of the central longitude and the frequency of occurrence are all modeled by the parameterization. The central latitude is also predicted, but this cannot be detected in Fig. 1. The stochastic component is easily detectable by the fact that there are notable differences among the three panels. The deterministic component is detectable via the fact that the amplitude and frequency of occurrence is notably larger during neutral and warm periods (i.e. January 1982–December 1984) compared to cold periods (i.e. January 1985–November 1986). The details of the state-dependent WWB parameterization are discussed next.

### 3.1. State-dependent WWB parameterization

This sub-section provides the details of the WWB parameterization. We also highlight some of the technical issues involved in including the parameterization in CCSM3 and CCSM4. The parameterization follows the work of Gebbie and Tziperman (2009). For our purposes WWBs are defined as zonal wind anomalies greater than  $5 \text{ m s}^{-1}$  that persist from 2 to 40 days, and with a zonal fetch of up to 500 km. We assume that WWBs can be modeled by a Gaussian in space and time (Luther et al., 1983; Fasullo and Webster, 2000; Yu et al., 2003; Eisenman et al., 2005). The zonal wind anomalies associated with WWBs are given as:

$$U_{\text{wwb}}(x, y, t) = A \exp \left( -\frac{(t - T_0)^2}{T^2} - \frac{(x - X_0)^2}{L_x^2} - \frac{(y - Y_0)^2}{L_y^2} \right) \quad (1)$$

The bursts are a function of temporal and spatial parameters; where  $A$  is amplitude,  $T_0$  is the time of peak wind,  $T$  is the event duration (persistence),  $X_0$  and  $Y_0$  are the central longitude and latitude, and  $L_x$  and  $L_y$  are the zonal and meridional fetch. Note that the probability of occurrence of a burst event does not appear in (1). This parameter is actually used as a trigger for both state independent and dependent WWBs. The only difference is that in the former, the probability is determined based on observed monthly climatology whereas in the later, it is strongly modulated by the low frequency variability of SST. The frequency of occurrence of the burst depends on SSTA in the state-dependent case, but the duration of the events remain constrained to be less than 40 days.

The spatial and temporal structure of each individual burst is computed as follows. The SVD modes of the SST decomposition with the wind stress are projected into the modeled SSTA to obtain projection coefficients, or PCs. These PCs are then projected into the regression coefficients of each WWB parameter (e.g. amplitude, zonal and meridional fetch, persistence, probability, and central latitude and longitude). The WWB climatology is added to this result to account for the observed seasonality dependence. Using the parameters noted above a burst is then constructed following Eq. (1). The addition of the WWB climatology is also done in the state-independent parameterization in order to be consistent with observations and with the state-dependent case. Once a wind burst is predicted to occur based on the parameterization (both state independent or dependent), the zonal wind anomaly is interpolated to the ocean model grid and converted to wind stress assuming a constant drag coefficient. The parameterization is applied as the coupled model evolves (e.g. interactively as the title suggest) and it produces a burst structure depending on seasonality (state independent case) and inter-annual SST structure (state dependent case). In other words, it is a fully interactive parameterization.

One difficulty in applying the WWB parameterization in the state-dependent case is that parameterization requires SSTA, whereas the model predicts total SST. This implies that as the CGCM is running model SST climatology needs to be identified. This is accomplished via an, anomaly coupling strategy (e.g. Kirtman et al., 2002). The anomaly coupling is only applied to the WWB parameterization – the model remains fully coupled in all other aspects. The second issue with this parameterization is that the SVD analysis is trained on observed SSTA and the modeled SSTA may well differ from observation.

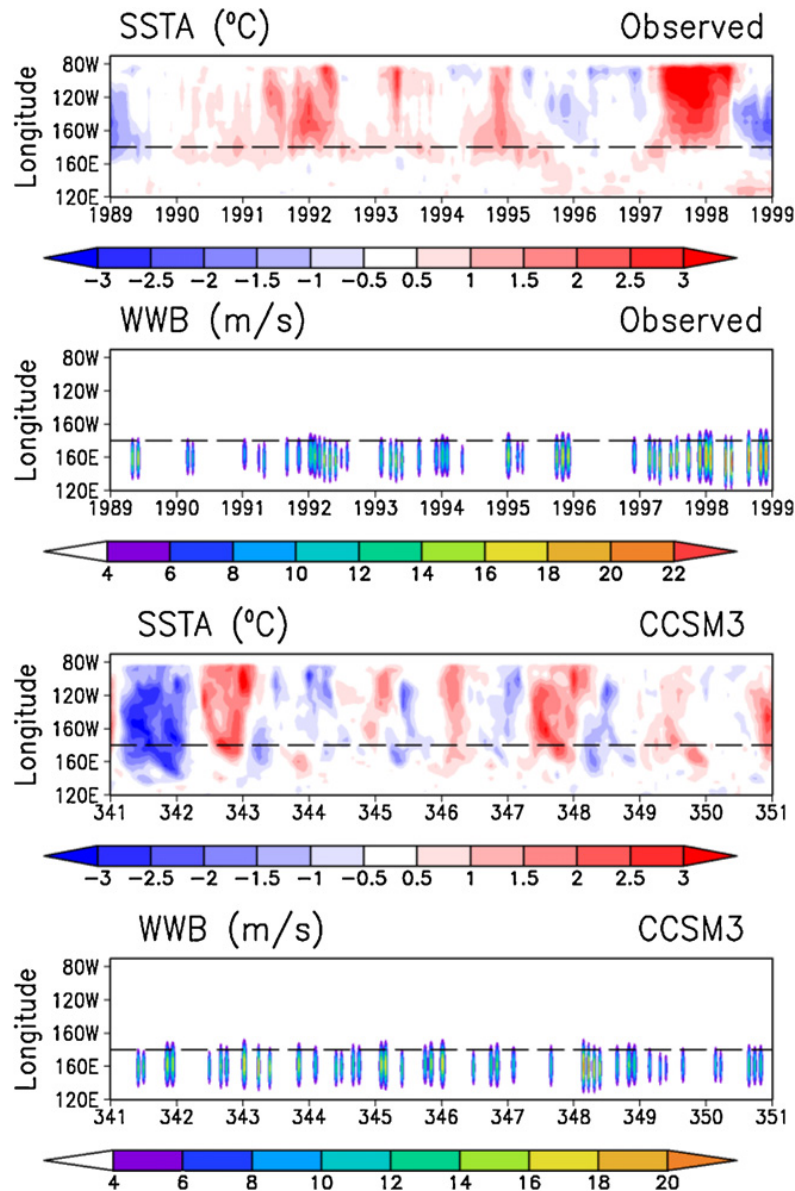


**Fig. 2.** State-dependent WWBs realization when using observed (top 2 panels) and CCSM3 (bottom 2 panels) SSTA. Time increment from left to right (~10 years) and longitude from bottom to top across the Pacific.

To demonstrate that the state-dependent parameterization here is suitable for this model, some WWB characteristics are plotted in Fig. 2 obtained using observed and modeled (CCSM3) SST anomalies. This figure is showing a time evolution of WWBs for 10 years period along the equatorial Pacific. The x-axis on all plots corresponds to time [in years]. The CGCM produce too frequent warm and cold events, affecting the periodicity of the wind burst due to its SSTA dependence. But, overall, all WWB parameters agrees with observation, especially those related to structure like central latitude, longitude (not shown), zonal, and meridional fetch. The amplitudes are also similar, with the exception of the very strong ENSO event of 1997/98. Based on these, we can say that the parameterization is suitable for this model.

#### 4. Observed versus parameterized WWBs

The purpose of this section is to further describe the observed characteristics of WWB and to compare to that obtained from the parameterization. First, we provide a brief description of how the bursts are extracted from observations. The wind data is the 1000 mb zonal wind from the NCEP/NCAR Reanalysis Project, expanding from 01 January 1948 to 31 December 2011. The data have a 2.5° by 2.5°

horizontal resolution and a daily time interval, same as the coupling interval of the ocean component of CCSM model. The data includes the tropical Pacific basin from 20S to 20N in latitude and from 120E to 80W.

Before describing how the observed WWBs characteristics are extracted from observation, the authors want to aware the reader that the PDF of the decoupled atmospheric variability in the western Pacific is closely Gaussian (with some asymmetry clearly linked to ENSO). So easterly anomalies have about the same probability to occur. The focus of this study is on their westerly portion only as the title suggest. The intent of this paper is to diagnose how the “observed” characteristics of westerly wind events affect ENSO statistics and dynamics. Essentially, we examine how atmospheric noise that has specific temporal and spatial scales and is geographically constrained impacts the model. This is in contrast to “non phenomenological” atmospheric noise that can be isolated with say, the interactive ensemble approach (e.g. Kirtman and Shukla, 2002). Other reason for limiting the noise to be just eastward is due to its relative importance in forcing equatorial SST variability. As demonstrated by studies sited in Section 1, WWBs are linked to tropical Pacific SST and appear to be state-dependent. Perhaps, the greatest motivation for this study is to investigate such state-dependence of WWBs on ocean state variables.

There are many definitions of WWBs in the literature; therefore, extracting these events from the zonal wind data is not trivial. Some WWBs definitions are listed in the following studies. For example, Harrison and Vecchi (1997) used anomalous surface winds relative to the monthly climatology to identify WWBs. Hartten (1996) used a WWB criterion in which 1000-hPa zonal winds exceeded  $5 \text{ m s}^{-1}$  with a zonal extent over  $10^\circ$  and lasting 2 days. On the other hand, Murakami and Sumathipala (1989) used bandpass-filtered 850-hPa zonal winds and identified WWBs with abrupt accelerations of westerly winds. Here, we will define WWBs in a way that is consistent with our state-independent and state-dependent parameterizations described earlier. The seasonal cycle is removed to produce a wind anomaly. Then, a wind burst is defined when:

1. Wind anomalies averaged from  $2.5^\circ\text{N}$  to  $2.5^\circ\text{S}$  lasts from 2 to 40 days.
2. The above condition has a minimum zonal fetch of 500 km.
3. Conditions 1 and 2 have anomalies exceeding  $+5 \text{ m s}^{-1}$ .

The meridional constrain imposed in condition 1 is chosen based on the known effect of WWBs on Kelvin wave excitation and amplification and in agreement with our WWBs parameterization (see Fig. 2). The 2–40 days frequency band is meant to include both, synoptic and intra-seasonal variability characteristics observed in WWBs. Condition 2 follows from 1 and the typical zonal scale in the tropics. Condition 3 is chosen so that a burst is defined when a total reversal of the Trade Winds occurs in the western Pacific, based on climatology. As any other definition of WWBs in literature, ours is empirical. Fig. 3 shows the observed WWBs according to our definition during the 1990s. All bursts are greater than  $5 \text{ m s}^{-1}$  as defined, with amplitude close to that of the state-independent case. Most of the bursts are clustered as a large-scale feature in the zonal direction with highly variable temporal structure. The majority of the observed WWBs occurred during the El Niño phase of 1992 and 1997, with weaker bursts in 1993 and 1995, consistent with the idea of the state-dependent formulation for the parameterization.

Our state-independent WWBs parameterization comprises of a stochastic component plus a seasonal cycle, whereas our state-dependent WWBs includes a deterministic component with interannual time-scale (tropical Pacific SSTA). The observed WWB has a strong interannual component. This feature is highlighted in Fig. 4 that shows a power spectrum of parameterized and observed WWB index defined by the area average from 140E to 160W and from  $2.5^\circ\text{S}$  to  $2.5^\circ\text{N}$ . Note that for all 3 cases, there is power at about  $\sim 0.1$  frequency band, corresponding to the seasonality of WWB. The state-independent bursts are largely white noise, but with a small hint of more power at high frequencies. Most of the power in the state-dependent and observation resides in the interannual band, especially that related to ENSO-like variability. For the observed case, this suggests a strong dependence on tropical Pacific variability.

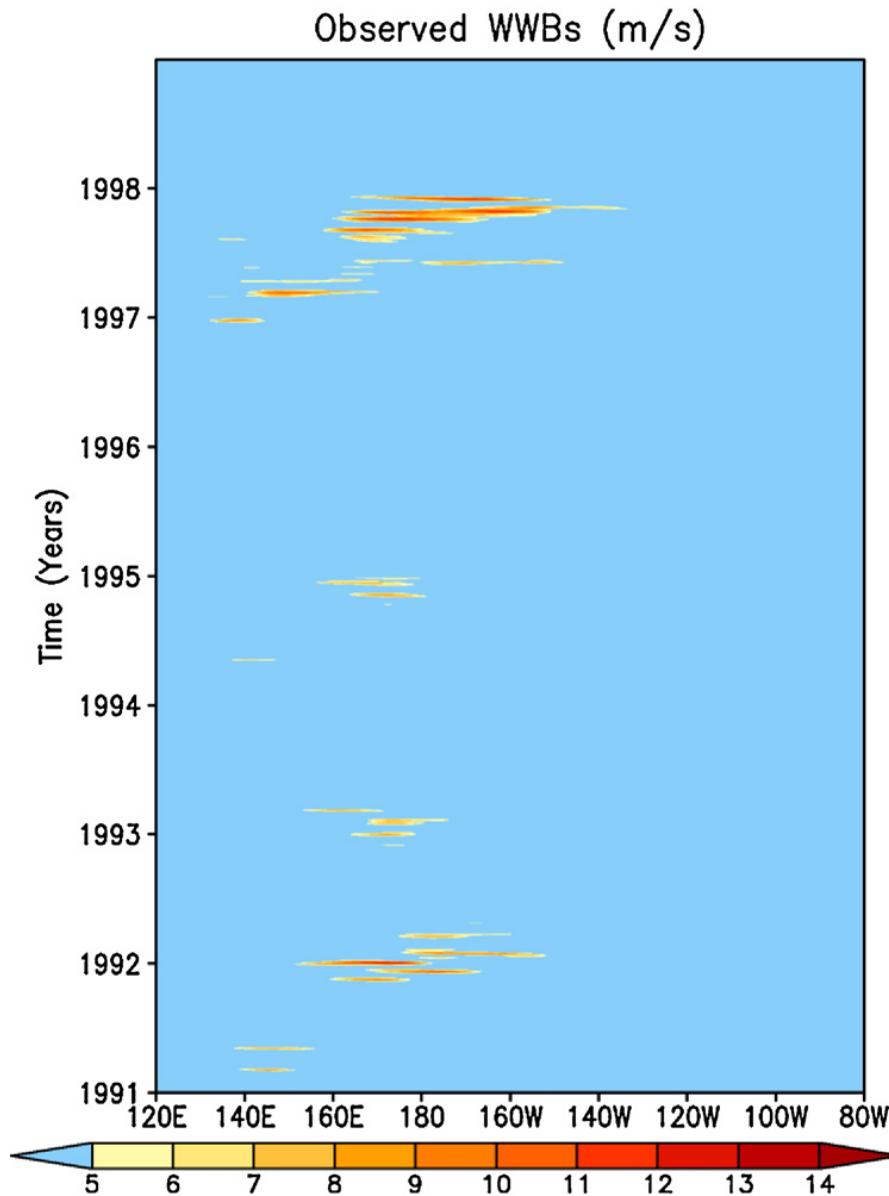


**Fig. 3.** Hovmoller diagram of observed WWBs ( $\text{m s}^{-1}$ ). Only showing a subset for the 1990s decade along the equatorial Pacific. Contours below  $5 \text{ m s}^{-1}$  are suppressed in blue. (For interpretation of the references to color in this figure legend, the reader is referred to the web version of this article.)

## 5. Results

We first discuss how the mean state and seasonal cycle are modified by the inclusion of state dependent and state independent noise. The long-term mean of ocean surface variables are largely unaffected by the different WWB parameterizations in these experiments. For example, Fig. 5 displays the Niño 3.4 annual cycle for our three experiments. It is very common for current Couple GCM to underestimate the seasonal cycle, or to have a dominant semi-annual component (Mechoso et al., 1995; Latif et al., 2001). First, it is important to remind the reader that CCSM3 has a well-known semi-annual seasonal cycle along the equator depicted in Fig. 5 (CCSM4 has an improved annual cycle, but this does not appear to impact how the parameterization affects the model). Using CCSM3, Pan et al. (2010) formulated an empirical heat flux adjustment that was able to simulate a more realistic mean state and seasonal cycle.

For all the experiments, the general time dependence of the annual cycle is unaltered. The state-dependent case has an overall warmer ocean surface, especially for the latter part of the year. The

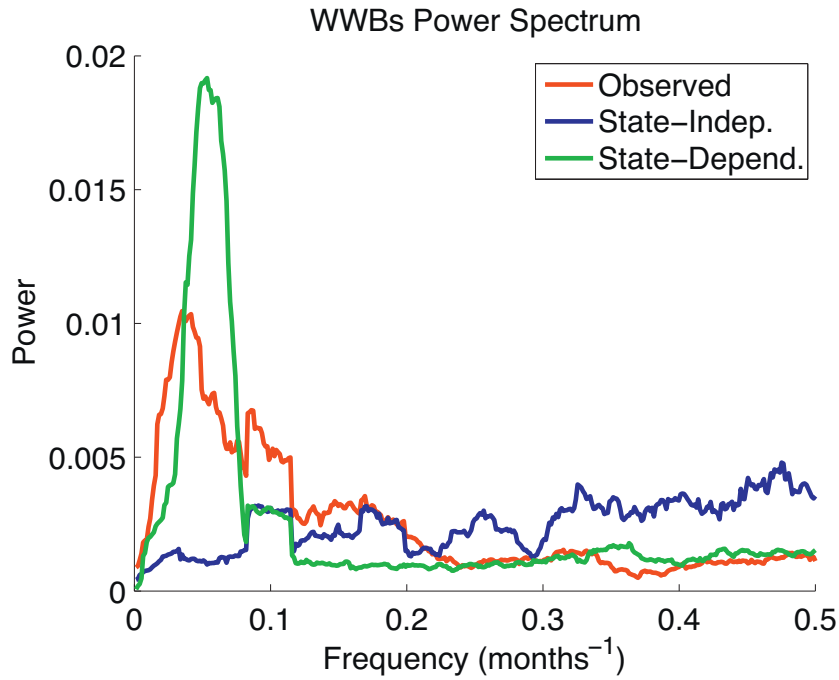


**Fig. 4.** Power spectrum of westerly wind burst index (area averaged from 140E to 180 longitude and 5S to 5N). Observed (red), parameterized state-independent (blue), and parameterized state-dependent (green). All parameterized burst are those coming out of CCSM3. Power in  $[\text{dyne/cm}^2]^2$ . (For interpretation of the references to color in this figure legend, the reader is referred to the web version of this article.)

warming does not appear to be important, since the maximum amplitude is only two tenths of a degree for the months of August and September. We believe that this difference has a relatively small influence on our results, and suggests that applying anomaly coupling for the WWB parameterization is a reasonable approach.

The time evolution of equatorial Pacific SST anomaly and the WWBs is shown in Fig. 6, for the control case. Note that the WWBs shown have been converted into a wind stress as applied in the

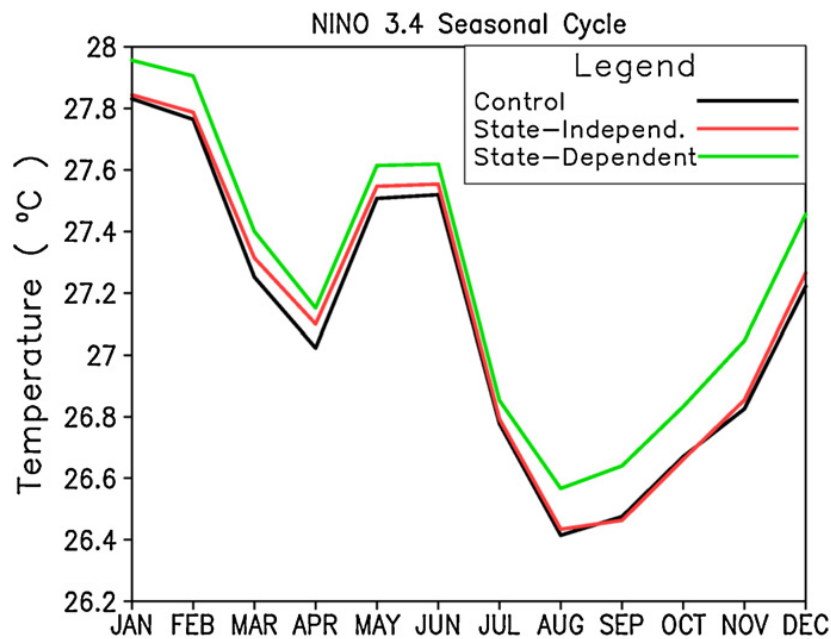


**Fig. 5.** CCSM3 Niño 3.4 SST seasonal cycle  $[\text{°C}]$ , control (black), state-independent (red), and state-dependent (green) experiments. (For interpretation of the references to color in this figure legend, the reader is referred to the web version of this article.)

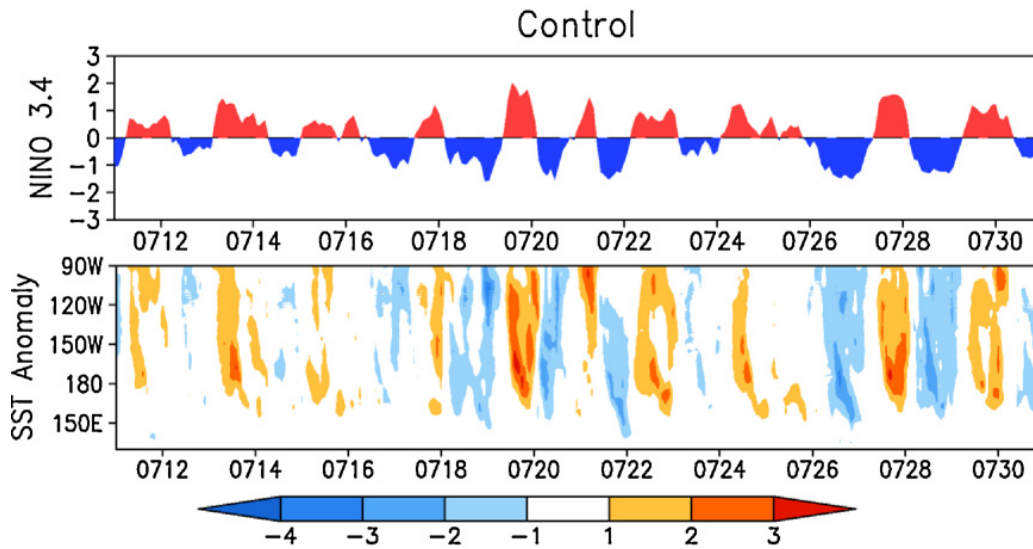


**Fig. 6.** CCSM3 control experiment time evolution of 20 model years of Niño 3.4 index  $^{\circ}\text{C}$  (top) and SST anomaly along the equator in  $^{\circ}\text{C}$  (bottom). X-axis represents time expanding 20 model years.

model (i.e. assuming a constant drag coefficient) and are in  $\text{dynes cm}^{-2}$ . Fig. 6 shows the Niño 3.4 index (top), sea surface temperature anomaly (SSTA) along the equator for the Pacific Ocean (bottom). These time series are taken randomly from 20 model years, but the time is consistent for all panels. Similarly, Figs. 7 and 8 describe these fields for the state independent and state dependent forcing cases respectively.

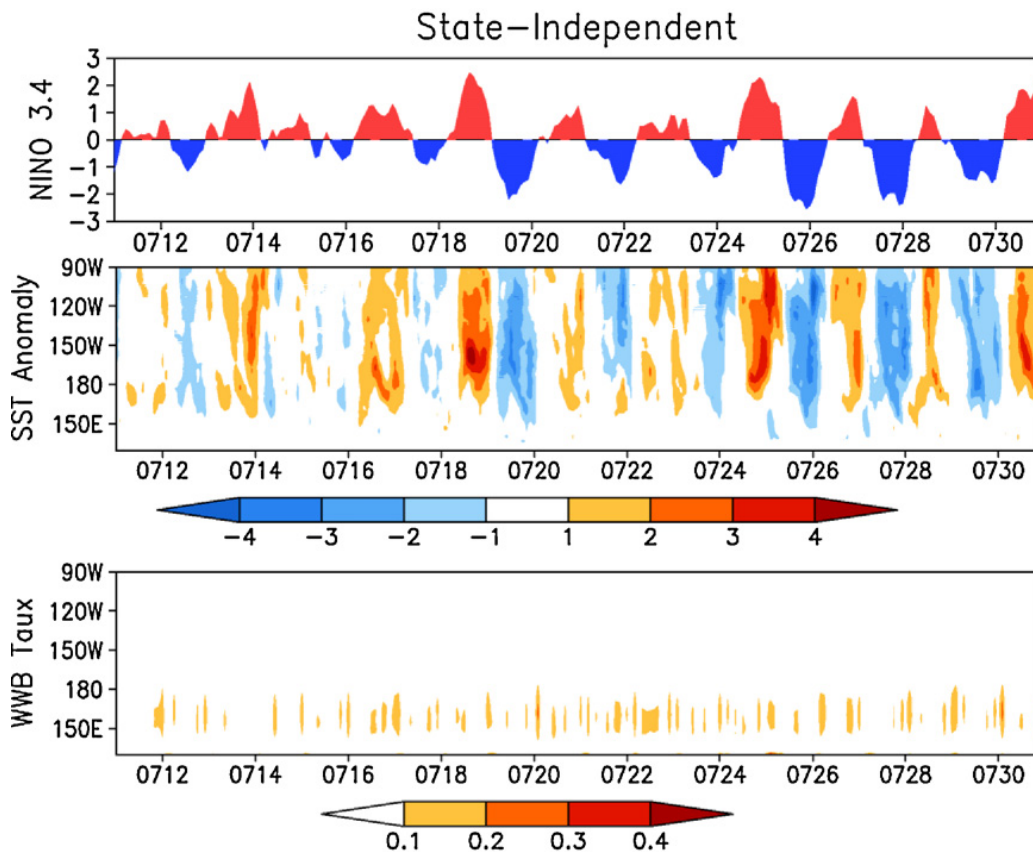


**Fig. 7.** Same as Fig. 6, but for the state-independent case. Also included, WWB [ $\text{dyne/cm}^2$ ] (bottom panel). The WWBs do not exceed  $0.2 \text{ dyne/cm}^2$ .

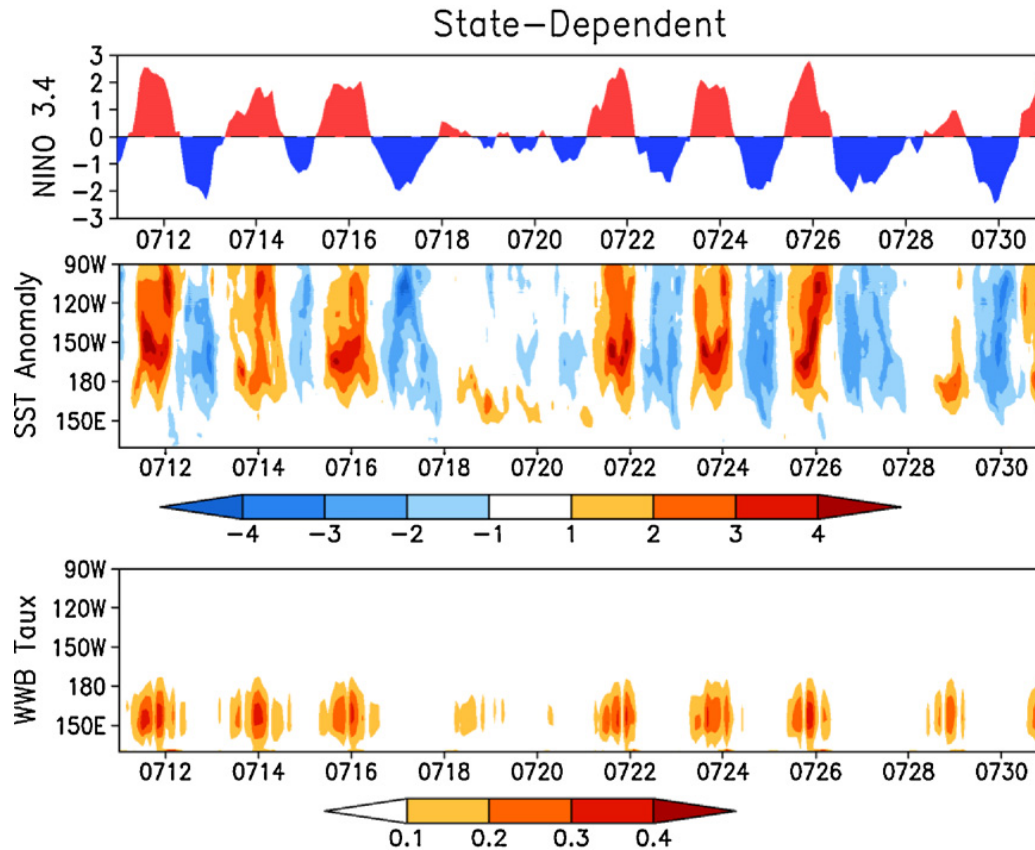


Fig. 8. Same as Fig. 7, but for the state-dependent case. Here, the WWBs exceed  $0.3 \text{ dyne/cm}^2$ .

There are no wind bursts in the control case (Fig. 6). In the state-independent case, the bursts are irregular in time (i.e. the probability of occurrence is about 4 bursts per year) but with little or no interannual variations (Fig. 7 bottom). Comparing this with the state-dependent case (Fig. 8 bottom), it is evident that the spatial and temporal characteristics of the WWB are modified by the coupling with the SST. In the state-dependent experiment, the WWBs are strongly coupled to the warm events. Despite the strong interannual variability it is important to keep in mind that seasonality still plays a role here, but it is relatively minor. See the previous section for more on the seasonal dependence of WWBs.

There are notable differences in the strength of the WWB for the state-independent and state-dependent forcing simulations. For example, it is evident that in the state dependent case the WWBs have larger amplitude than in the state-independent parameterization. This is due to positive atmospheric feedback in that the WWBs increase the amplitude of the warm SSTA, which in turn increase the WWBs. The positive feedback works as follows. Since our WWBs are centered at the equator, they will force downwelling Kelvin waves that will propagate eastward producing a warm SSTA in the eastern Pacific. This SSTA will reinforce atmosphere convection, strengthening the westerlies, which will have a positive feedback on the SSTA. Apparently there is no difference in the location of the warm pool edge among the three cases, therefore, the ocean advection feedback is not playing a role in the strengthening of the bursts in the model. From Fig. 8, it is also evident that there is a high correlation between the WWBs and the SSTA in the central and eastern Pacific; this will be further analyzed in this section.

Comparing the SSTA for the three cases (Figs. 6 bottom and 7 and 8 middle) there appears to be evidence of a reduction of the bias toward more cold events in the state-dependent case with respect to the control case. This issue will also be discussed later in this section. The amplitude of ENSO events also appears to increase in the state-dependent case, but no doubling in intensity as seen Eisenman et al. (2005). This may be because our WWBs are state-dependent and they were completely deterministic in Eisenman et al. (2005). The experimental design and the models used are quite also different.

**Table 1**

CCSM3 December–January–February (DJF) averaged Niño3.4 SSTA, number of cold (a) and warm (b) events out of 201 model years. Magnitude (threshold) given in column 1 [ $^{\circ}\text{C}$ ].

	$^{\circ}\text{C}$	Control	State-Ind.	State-Dep.
a)				
	<−1.00	40	30	61
	<−1.25	32	23	52
	<−1.50	22	15	40
	<−1.75	13	8	34
	<−2.00	7	7	21
b)				
	>1.00	41	31	73
	>1.25	22	16	61
	>1.50	9	6	48
	>1.75	2	3	22
	>2.00	1	1	4

To quantify the reduction of the cold bias, we count how many ENSO events, in both extremes, were observed during 201 model years. These events were also separated into different strengths. Table 1a shows the December, January, and February (DJF) Niño 3.4 (area average from 170E to 120E and 5S to 5N) extreme cold events count for 201 model years. The first column is the amplitude of the cold events in degrees Celsius. Table 1b is in the same format but for warm events. The state independent noise forcing case produces about 25 percent less ENSO overall when compare to the control run (excluding the very extremes), this reduction is yet not well understood, but does indicate a more peaked distribution with weaker tails. The state dependent WWBs forcing experiment produces more ENSO events in both phases. This is true for all magnitude events, which can be seen by comparing the values horizontally in Table 1. For the very extreme warm (cold) events, the ratio of the number of events in the control to the number of events in the state dependent WWBs forcing experiment is 1/4 (1/3).

The state dependent WWBs experiment appears to reduce the bias toward more cold than warm events as in the control. This can be detected by comparing cold versus warm events of similar amplitudes in Table 1. The ratio of cold to warm events (greater than 1  $^{\circ}\text{C}$ ) is about one for the control and state-independent cases, while is about 0.83 for the state-dependent. Only in the very extreme cases, the La Niña phase dominates, with a ratio of 5.25 of cold to warm extremes. This ratio is 7 for the control and the state-independent cases. As a result, we argue that there is a shift from an ENSO that is episodic or event driven to more of an oscillation as the experiments progress from the control to the state dependent WWBs case. That is, in the state-dependent case, the number of ENSO neutral winters (i.e. December–February Niño3.4 SSTA less than 1  $^{\circ}\text{C}$ ) is similar to the number of ENSO active winters (i.e. either warm or cold), suggesting that the system has become more oscillatory.

A histogram of the Niño 3.4 SSTA is shown in Fig. 9. Also, the second, third, and fourth statistical moments are shown with their respective 99% confidence interval obtained by a statistical bootstrapping procedure. No significant differences are observed between the control and the state independent forcing cases, only that the later displays a more peaked distribution. This is consistent with Table 1, which indicated fewer extreme events in the state-independent case compared to the control (or the state-dependent simulation). The control and the state-independent cases have similar skewness, but the second (fourth) statistical moment is smaller (more positive) for the later.

There are, however, notable differences between the state dependent stochastic forcing and the control (or state independent stochastic forcing) simulations. For example, the standard deviation is larger and kurtosis is more negative suggesting an increase in ENSO event count. Also a closer to zero skewness coefficient than in the control or state independent case, depicting a reduction in the cold bias (or the ratio of cold over warm events). Note that the third moment remains negative, due to the very strong cold events, which for this state-dependent case, sometimes exceed  $-3^{\circ}\text{C}$ . The still negative skewness is a product of the overwhelmingly dominating cold event at magnitudes greater than 1.75  $^{\circ}\text{C}$ . That is, there are more cold than warm events at this amplitude, producing a longer left

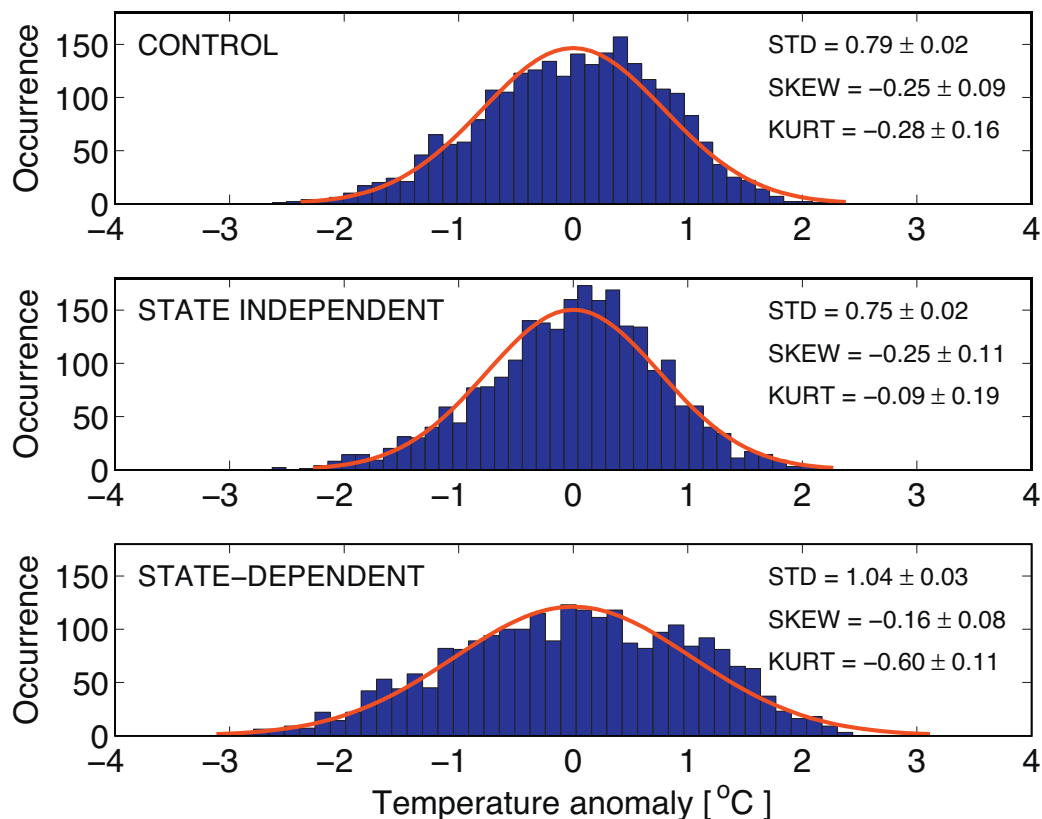


**Fig. 9.** CCSM3 histograms of Niño 3.4 SSTA for 201 model years. Control (top), state-independent (middle), and state-dependent (bottom). Normal distribution fitted (red). The y-axis represents the occurrence (in months). Also showing standard deviation, skewness, and kurtosis coefficient plus their statistical significance at a 99% confidence level. (For interpretation of the references to color in this figure legend, the reader is referred to the web version of this article.)

tail in the histogram. Consistent results are obtained by analyzing wind stress anomaly on the central Pacific (not shown).

Thus far, we have shown that state-dependent noise in the form of WWBs modifies some of the broad ENSO statistics. Here we examine how the parameterized WWBs affect ENSO dynamics and its spatial characteristics. For example, Fig. 10 depicts tropical Pacific SST standard deviation for observed, control, state-independent, and state-dependent case. Some of the well-known CCSM3 biases described in the previous sections can also be detected here. Comparing the control case with observation there is a clear confinement of SST variability about the equator in the model. This is especially true in the eastern portion of the basin. Another discrepancy with observation is the location of maximum variability. The model has variability that is too strong in the far western Pacific this is associated with a too shallow thermocline and the lack of thermocline plateau in the warm pool region. There is a small reduction in the standard deviation for the state-independent case as compared to control. Surprisingly, most of the differences are over the eastern part of the basin, while this decrease in variability is small, it is statistically significant as described in Fig. 9. This may be hinting that state-independent noise actually damps ENSO in this model (stochastic forcing in already chaotic systems can be shown to damp variability; see Siqueira and Kirtman, 2012). On the other hand, state-dependent noise increases the interannual variability. The enhancement occurs throughout the basin, with a strong impact over the Niño3.4 region. Overall, there are no significant changes in the horizontal structure but only in the amplitude of variability.

To diagnose the impact on ENSO dynamics we also examine correlations between state variables and the WWBs. The correlation of sea surface temperature (SST, shaded) and a WWBs index (the area average of WWBs from 5S to 5N and from 140E to the date line) is shown in Fig. 11 (shaded). Similar, but for sea surface height (SSH) and WWB index is depicted by contours. The control run is not shown since it does not have WWBs. We see that there is no correlation between SST and the WWBs for

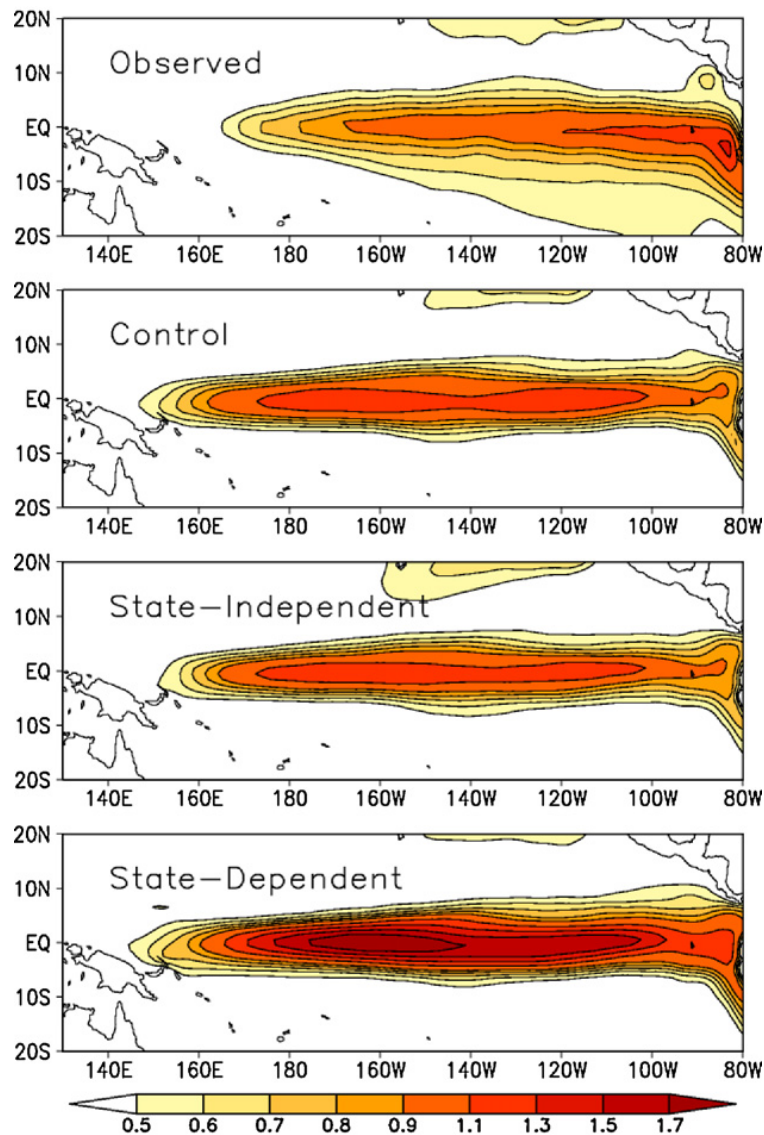


**Fig. 10.** Tropical Pacific SSTA standard deviation [ $^{\circ}\text{C}$ ] for: observed and CCSM3 control, state-independent, and state-dependent case.

the state-independent case (Fig. 11 top). This result is somewhat of a surprise. One possibility could have been that the additive WWBs served to increase the amplitude of an ongoing warm event. If this were robust, we would expect to see some WWB activity for the strongest warm events. Our analysis indicates that there is no relationship at all between state-independent bursts and tropical Pacific interannual variability.

High correlation is observed in the state-dependent case (Fig. 11 bottom), from about the central longitude of the bursts eastward. Some negative correlation is detected in the western Pacific off equatorial region. Similar patterns are observed for the sea surface height (contour) and zonal wind stress (not shown). Any weak correlation that is detected between any of these state variables and the WWBs in the state-independent case is the result of local air–sea interaction, especially in the SSH. For the multiplicative forcing case, the WWBs are positively (negatively) correlated with SSH anomaly in the eastern (western) Pacific, linked through SST anomaly by state dependence in the WWB parameterization. We also detect some off-equatorial signal in the SSH (contour), which suggest the potential importance off-equatorial wave activity.

In terms of the SSH variance (Fig. 12), some basic differences among the experiments are observed, but the overall spatial distribution of regions with high variance (regions inside a box) are similar. Along the equator in the central Pacific (approximately the Niño 3.4 region), the variance is due

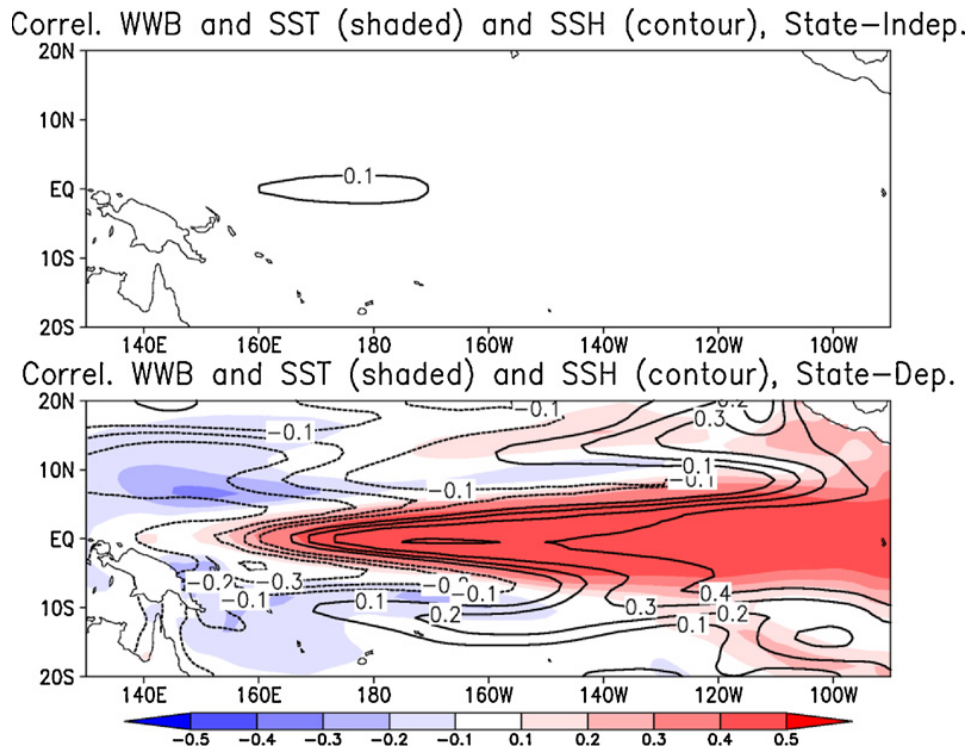


**Fig. 11.** Correlation of SSTA (shaded), SSHA (contour) with a WWB index (WWB average over 140–180 longitude and 5S–5N latitude), state-independent (top) and state-dependent (bottom). Results are for CCSM3.

to equatorial Kelvin waves, whereas those off the equator are due to Rossby waves (i.e. regions 2 and 3). Given the importance of equatorial wave dynamics in modulating ENSO, we examine the correlation of some state-variables with Niño3.4 region. Fig. 13 shows the lag-lead correlation of SSH anomaly (shaded) along the equator with SSTA index in Niño3.4 region of Fig. 12. Similarly, the SSTA (contour) is also shown. We note that the Niño3.4 region is strongly correlated with SSHA along the equator, especially east of the date line. This is clearly shown in Fig. 13 at zero lag. The correlation analysis suggest that state-dependent parameterization enhances lag-lead coherence in correlation, again supporting the assertion that state-dependent noise drives the system away from an episodic ENSO to a more oscillatory ENSO. This increased lag-lead coherences is also seen when examining the correlation along 7° North (not shown) with the only difference in phase speed (slower than at the equator) and direction of propagation (westward). Correlation is strongly reduced by the state-independent WWBs implementation as compared to control, especially at lags. This is a surprising result given that ENSO statistics itself did not change much when the bursts are state-independent.

As further evidence for the increase temporal coherence in state-dependent case, we perform a composite analysis of ocean surface variables and the parameterized WWBs. Fig. 14 shows a multi-year lag-lead composite of SSTA, SSHA, and WWB averaged from 5S to 5N along the equatorial Pacific Ocean for the control (left), state-independent (center), and state-dependent (right) cases, respectively. The composite includes the top 5 warm events based on Niño 3.4 SSTA centered at time zero lag. These 5 top events are chosen based on the Niño 3.4 index for December–January–February (DJF) average. To the far right of Fig. 14 is a time series composite of the WWB index (140E to 180 longitude and 5S to 5N latitude) for state-independent (black line) and state-dependent (red line) case. The relatively weak composite WWB amplitude in the state independent case suggests that strong WWBs are not indicative of strong ENSO events (see also Fig. 15). Conversely, strong WWBs are coupled to strong warm events in the state dependent case. The composites suggest that the state-independent case is even less oscillatory (or more damped) than the control simulation. The state independent noise reduces the lag-lead temporal coherence of the ENSO events. For instance, lag and lead SSH anomalies are notably weaker than in the control simulation. The SSTA

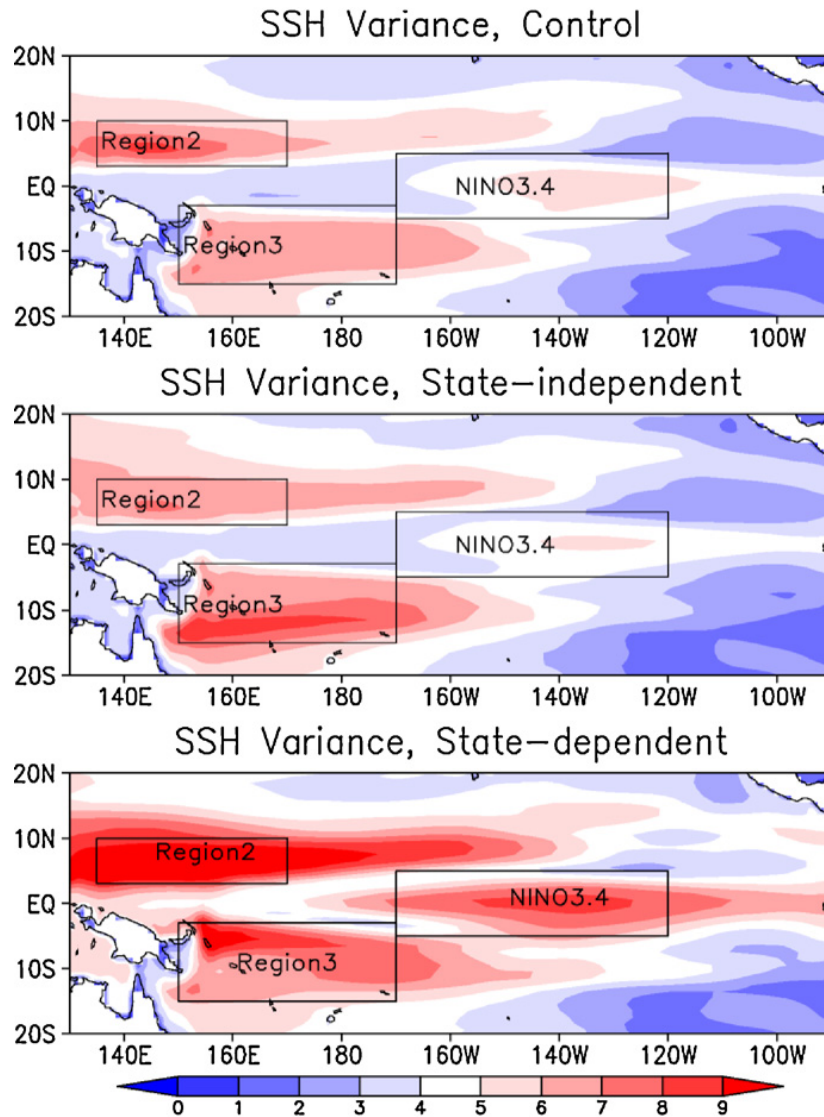


**Fig. 12.** Sea surface height (SSH) variance [ $\text{cm}^2$ ] across the tropical Pacific, control (top), state-independent (middle), and state-dependent case (bottom). Results are for CCSM3.

are confined to relatively small lags and leads where the composite apparently has little or no SSTA precursors.

In the state-dependent case (Fig. 14) the lag-lead composite suggests a considerably stronger oscillatory behavior. This is also supported by the lag-lead correlation shown in Fig. 13. The biennial ENSO period is also captured by this composite. Moreover, Fig. 14 shows the eastward propagation of SSHA clearly depicted throughout the composite at all lags. The WWB cycle shows a strong interannual dependence due to its coupling with the SST, but the annual cycle dependency of the WWBs is difficult to detect given the larger interannual signal. In the case of the state dependent composite there is a clear oscillatory pattern as a precursor to the strongest warm events. However, once the strong warm event has occurred there is little post event signal. This behavior is not only seen in SST and SSH but also in the WWB amplitude. There appears to be a low frequency build-up or development for the strongest warm events in the state dependent case that is not detected in either the control or the state independent case.

The above lag-lead correlations and composites are based on the state of ENSO. Alternatively, here we examine composites based on the parameterized wind bursts. Fig. 15 shows the composite for the state-independent (left) and dependent (center) case and the bursts (right). Note that the SSTA and SSHA are very weak even at 0-lag for the state-independent case. Again, indicating the state

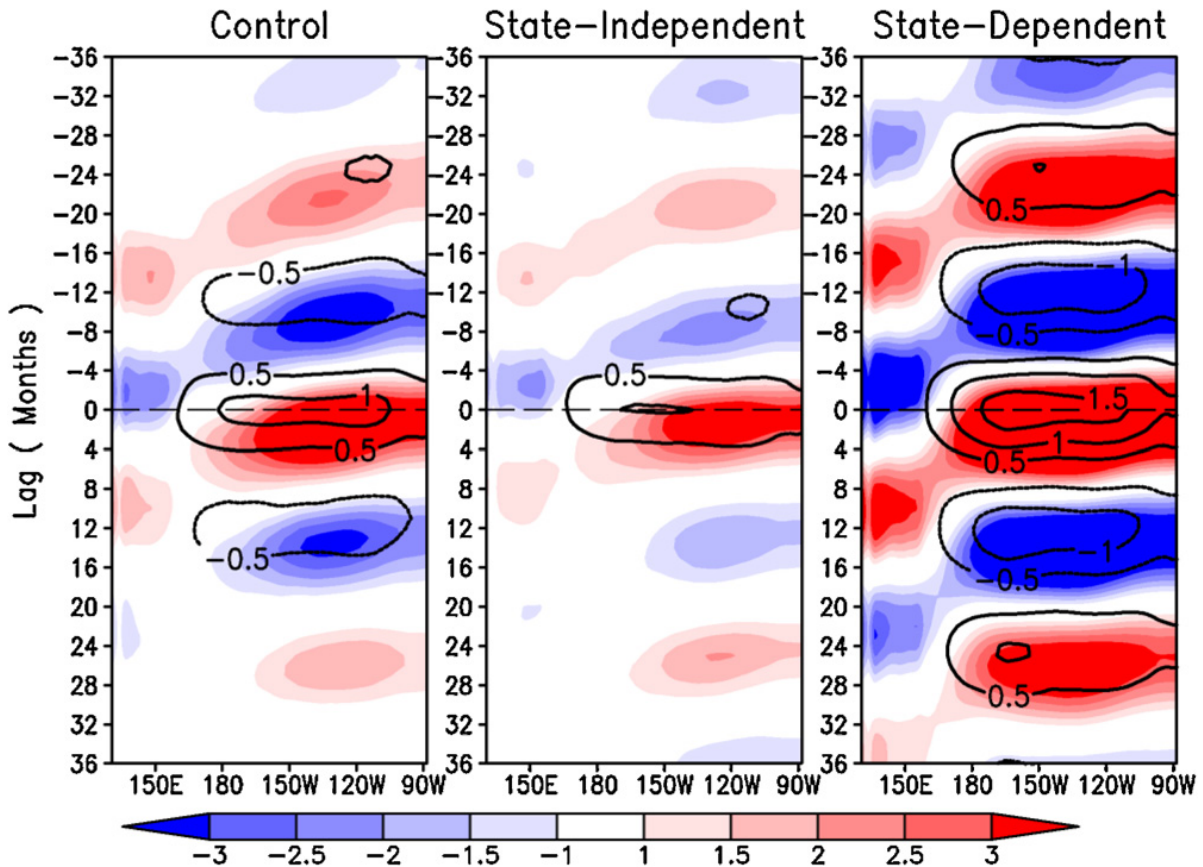


**Fig. 13.** Lag-lead correlation of sea surface height anomaly (SSHA) along the equator (shaded) and sea surface temperature anomaly (SSTA, contour) with Niño3.4 SSTA index. Positive lag means that Niño3.4 lags by as many months. Horizontal axis depicts longitude and vertical axis describes lags (months).

independent bursts are not particularly correlated with the strength of the warm events. The SSHA only shows a small local response to the westerlies a few months after they occur. This is due to local Ekman pumping produced by the positive zonal wind stress along the equator. It is also clear that the burst centered at 0-lag is the strongest (black line), but its persistence in time is short compared to the state-dependent case. As expected for the state-dependent case, there are no precursors associated with the WWB composite. The parameterization is localized in time. However, the state dependent WWBs do seem to have considerable lead-time coherence. From lag-0 up to leads of 36 months the increased oscillatory nature of the simulation is detected in both the SSHA and the SSTA. This further supports the hypothesis made earlier that WWB (state-dependent) can shift the system to a more oscillatory regime.

The decrease (increase) in SSH west (east) of the burst is evident in Fig. 15 (middle). The strongest height anomaly occurs two years after the strongest bursts. This is true not only east of the Dateline, but also on the western portion of the basin, where very strong positive anomalies are present. Similar to our lag-lead correlation analysis, these SSHA in the western basin propagate eastward, reaching the central (eastern) part of the basin in about 6 (9) months. This may be important in ENSO forecasting using this model given that SSHA can be a precursor to warming in the eastern part of the basin. Fig. 15 is a clear example of how the state dependent noise can drive ENSO from an episodic event regime to a self-sustain oscillatory regime.

The strongest SSTA variability is located over the central Pacific basin (180–140W) for all cases. This is the result of errors in the model, and although we have not completely diagnosed these errors, at least some of this problem is due to mean state biases. For the state-dependent case, SSTA variability increases throughout the basin, especially over the central Pacific. In contrast with control and state-independent cases, SSTA variability is enhanced over the eastern basin (east of 120W) when the WWBs

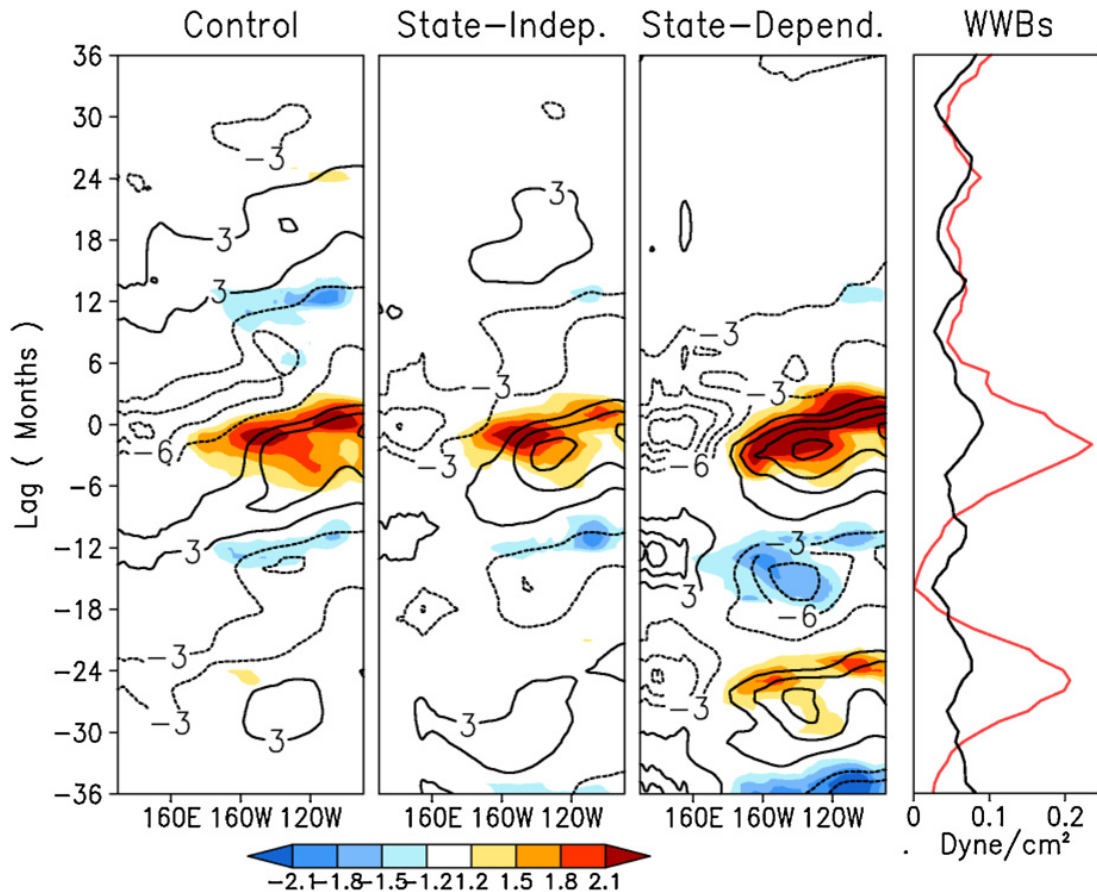


**Fig. 14.** Composite of top 5 (strongest) ENSO warm events for control, state independent, and state dependent case. Sowing sea surface temperature anomaly (SSTA) in [ $^{\circ}\text{C}$ ] (shaded) and sea surface height anomaly (SSHA) in [cm] (contour) across the equator averaged from 5S to 5N. Also showing WWB composite (right) in [ $\text{dyne}/\text{cm}^2$ ] for state independent (black) and dependent (red). Composites are based on December–January–February (DJF) Nino3.4 index, defined by area-averaged SSTA from 170W to 120W longitude and 5S to 5N latitude. (For interpretation of the references to color in this figure legend, the reader is referred to the web version of this article.)

depend on SST. A possible reason for this is that the effect of downwelling Kelvin waves, forced by WWBs, on SSTA counteracts some of the local cold bias. A composite analysis of potential temperature across the Pacific and at depths (not shown) is performed. For the state-independent case, we note that both warm and cold ENSO events have about the same magnitude as the control. There are weak signal over the central Pacific were state-independent warm events are slightly warmer ( $\sim 0.4^{\circ}\text{C}$ ). The thermocline depth is remarkably similar for both cases during warm and cold events. On the other hand, for the state-dependent case, both warm and cold events have greater amplitude. During warm events, there is significant reduction of the zonal thermocline gradient. Such reduction is associated with downwelling Kelvin wave forcing by WWBs and it has a greater impact over the far east where there is a deepening of a about 50 m as compared to control. We argue that equatorial wave dynamics is playing a significant role in the enhanced variability due to state-dependent WWBs, but a significant part of its effect over the far eastern portion of the basin is counteracted by the mean state bias in that region.

## 6. Model sensitivity

Arguably, CCSM3 has a flawed ENSO and annual cycle and it is possible that these errors affect the interaction between the model ENSO and the parameterized WWBs. Here we examine some elements of model dependence by introducing the WWB parameterization into CCSM4, which is known to have a significantly improved ENSO and annual cycle. In this section, only the most critical results described earlier are recreated. One reason is that the CCSM4 runs are relatively shorter,

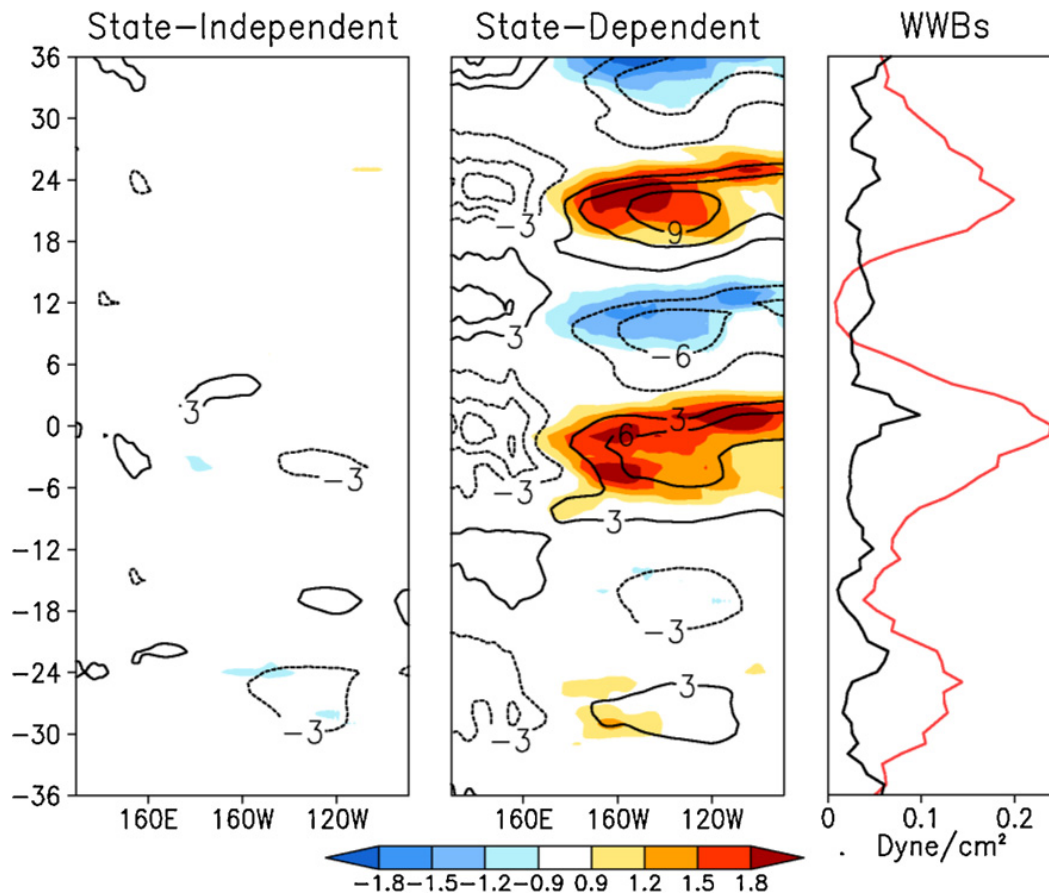


**Fig. 15.** Composite of top 5 (strongest) WWBs events for state independent (left) and state dependent case (center). Sowing SSTA in [ $^{\circ}\text{C}$ ] (shaded) and SSHA in [cm] (contour) across the equator averaged from 5S to 5N. Also showing WWB composite (right) in [ $\text{dyne}/\text{cm}^2$ ] for state independent (black) and dependent (red). Composites are based on WWBs index, define by area-averaged bursts from 140E to 180 longitude and 5S to 5N latitude. (For interpretation of the references to color in this figure legend, the reader is referred to the web version of this article.)

about 100 years, and because we used a coarser resolution model. The lower resolution for CCSM4 was chosen based on computational time constrain. The aim of this section is not to make model-to-model comparison, but to examine whether the differences observed among experiments are model dependent.

First, we examine the interannual variability in the tropical Pacific. Fig. 16 shows SST standard deviation for observed, control, state-independent, and state-dependent case, similar to Fig. 10 but for CCSM4. The SST variability in the eastern basin are closer to observations in this model than in its previous version, but the excessive variability in the western Pacific remains. Some modest increases in the meridional scale of the SSTA can be detected. In contrast with CCSM3, some enhancement in variability is observed for the state-independent case, especially in the cold tongue region. There is also a widening in the north-south direction of the variability for both parameterizations, which was unobserved in the case of CCSM3. For the state-dependent case, there is significant amplification of SST variability throughout the basin, consistent with CCSM3. Overall the biggest contrast between the models is in the state-independent case.

In order to compared the WWB parameterization between CCSM3 and CCSM4, correlation of SST (shaded) and SSH (contour) with a WWB index are shown in Fig. 17. The index, as before, is the area averaged bursts from 140E to 180 longitude and from 5S to 5N latitude, this is the same as Fig. 11 from CCSM3. Again, the control case is not shown (e.g. no WWB). Consistent with CCSM3, there is little or no correlation between the state-independent bursts and state variables as expected. On the other hand, a clear large-scale pattern emerges in the correlation pattern for the state-dependent case. Note that both SST and SSH depicts the structure observed during warm ENSO events. There are notable

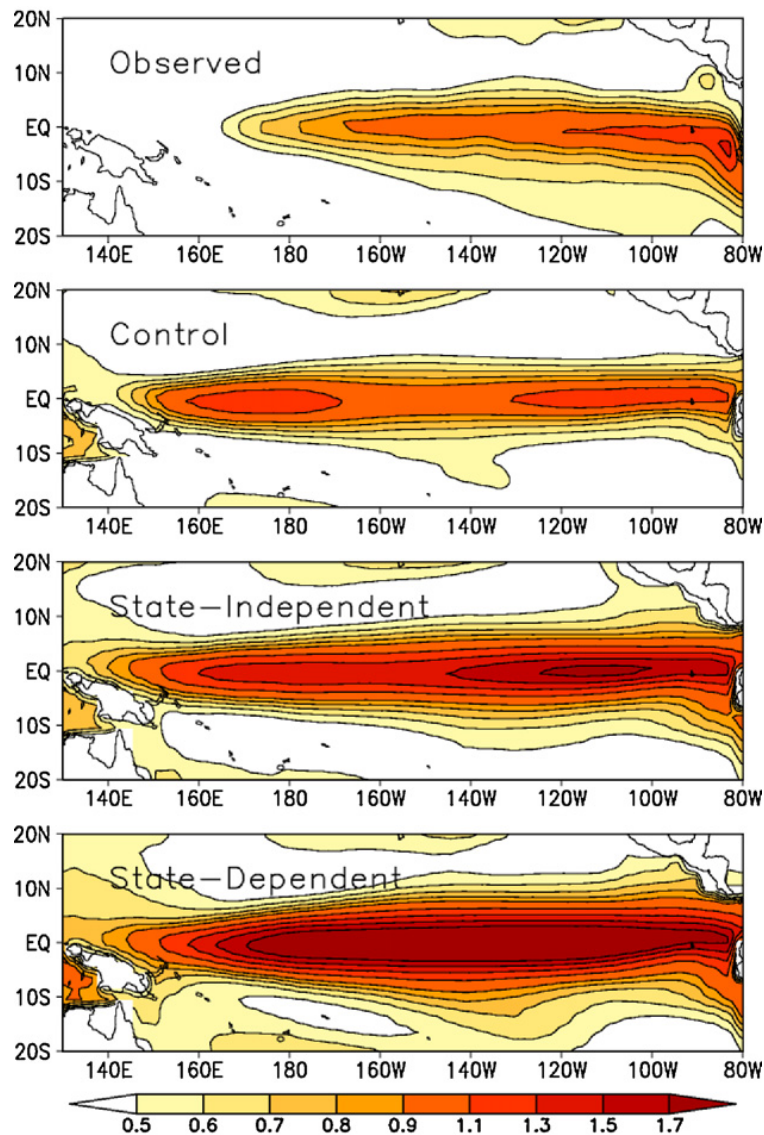


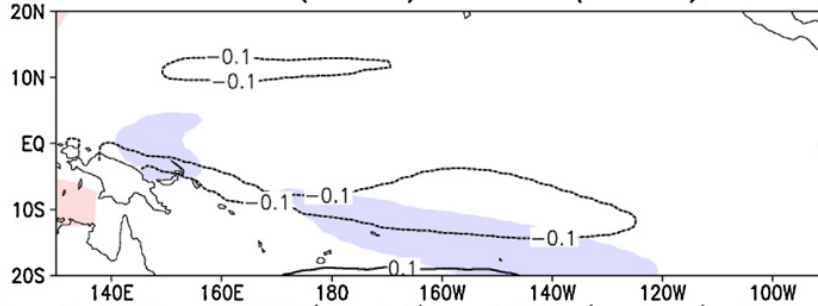
Fig. 16. Same as Fig. 10 but for CCSM4.

differences between this figure and that associated with CCSM3. In particular, the meridional structure in SST is considerably broader in CCSM4, which is consistent with the longer ENSO period. Such difference is analogous to the contrast of inter-annual variability between the two models, where in CCSM3, SST anomalies are confined close to the equator. Another difference of note is in the amplitude of the correlation. It is unclear whether such changes are attributed to different ENSO dynamics between the models, or differences in resolution.

Now, let's concentrate on how ENSO dynamics is modified by both WWB parameterizations in CCSM4. For this, the lag-lead correlation is repeated but for CCSM4 (i.e. compare Figs. 13 and 18). Note that Fig. 18 is the same as Fig. 13 except that longer lags and leads are included consistent with a longer ENSO period. Similar to CCSM3, adding state-independent WWBs has little detectable impact. In the state-dependent case, an enhanced oscillatory pattern is observed, as was found with CCSM3. These results suggest that some of the broad qualitative effects of the WWB parameterization are model (version) independent at least in the context of CCSM.

To further illustrate the impact of the parameterization in both models, a power spectrum of Niño3.4 SST anomalies is shown in Fig. 19. The SST index is obtained from the first principal component (PC) of an EOF analysis of tropical Pacific SST. EOF1 describes variability associated with that of ENSO. The power spectrum calculation was also performed on just SST anomalies for the Niño3.4 region and the results were very similar to that obtained from PC1. Fig. 19 includes all three cases from

Correl. WWB and SST (shaded) and SSH (contour), State-Indep.



Correl. WWB and SST (shaded) and SSH (contour), State-Dep.

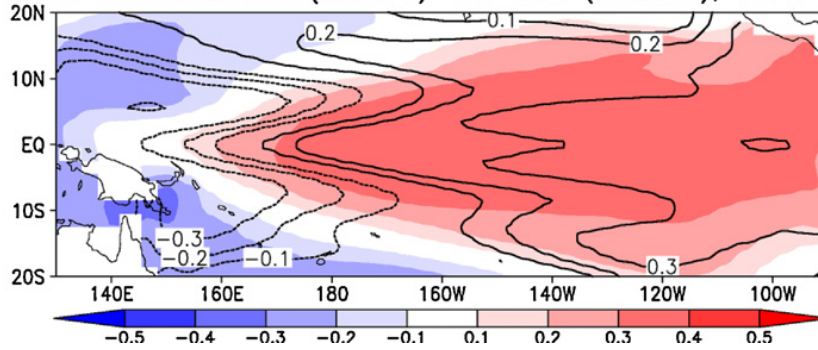


Fig. 17. Same as Fig. 11 but for CCSM4.

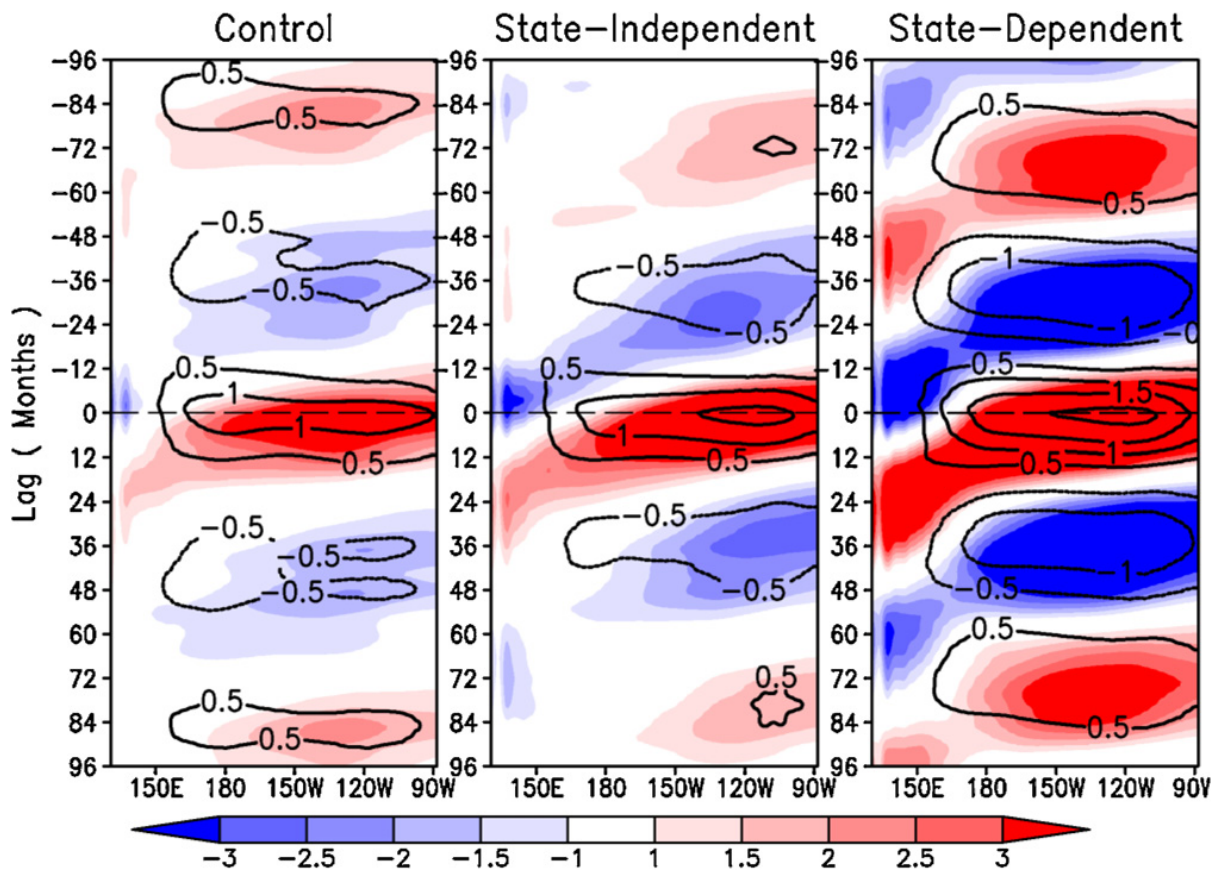
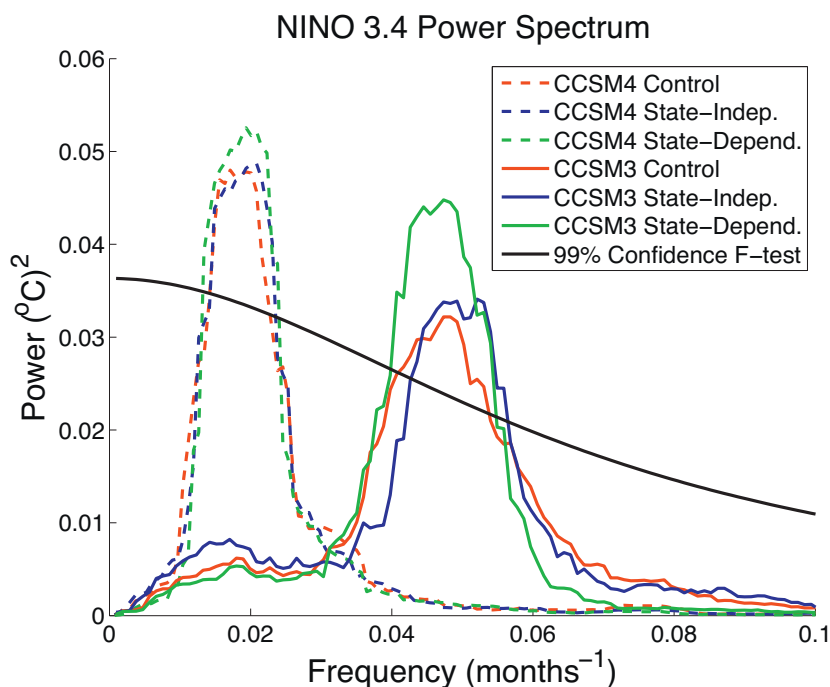


Fig. 18. Same as Fig. 13 but for CCSM4.



**Fig. 19.** Power spectrum of Nino3.4 SST anomaly reconstructed from the 1st EOF of tropical Pacific SST. Showing CCSM3 (solid) and CCSM4 (dashed). Control experiments in red, state-independent in blue, and state-dependent in green, 99% *F*-test confidence level (black). (For interpretation of the references to color in this figure legend, the reader is referred to the web version of this article.)

CCSM3 (solid) and CCSM4 (dashed), with the 99% *F*-test confidence level (black curve). This clearly shows the quasi-biennial ENSO period in CCSM3 and the longer period in CCSM4.

Comparison on Fig. 19 is only made for those frequency bands that pass the *F*-test. These include the periods of 18–26 months (CCSM3) and 42–78 months (CCSM4). In both models, there is little difference between the control (red) and state-independent (blue) case. Only a slight shift toward higher frequencies is detected in the state-independent. For the state-dependent case (green), a clear increase in power is observed for both models. There is also a slight widening of the power band at ENSO frequencies. This becomes more obvious when looking at the area under the curve bounded by the confidence *F*-test line. An increase power in those frequency bands is also an indication of enhance oscillatory behavior, as was shown with lag-correlation and composite analysis in previous sections. Both models show similar sensitivity to the inclusion of both the state independent and state dependent WWB parameterization. For CCSM4, the difference between state-dependent and control appears to be less than in CCSM3. This is because for the former model, the curves are located at lower frequencies. In reality, the area under the curve for both model are increased consistently by the inclusion of state-dependent noise.

## 7. Summary and discussion

This work was motivated by the need to understand how sub-seasonal variability potentially interacts with interannual variability. Our target or case study focused on WWBs, and we introduced westerly wind burst anomalies in CCSM3 as state dependent and state independent stochastic forcing. This is the first time that a state dependent and state independent WWB parameterization has been incorporated into a state-of-the-art coupled general circulation model.

We showed that state independent WWBs had only a minimal impact on the mean state or the interannual variability, while state dependent noise modified both, although the impact on the mean was relatively small. For example, a slightly warmer tropical central Pacific climatology was obtained in the state-dependent forcing experiment, but the phase of the annual cycle was unchanged from the control case and the warmer SST do not appear to have impacted the results described here.

To provide some assessment of model dependence in these broad-brush results we also applied the parameterization to CCSM4, albeit at lower spatial resolution.

Perhaps, the most striking result presented here was the fact that the state-independent WWBs had a minimal effect on the overall variability in CCSM3 and CCSM4. This is consistent with Zebiak (1989), using a simplified or intermediate coupled model of the tropical Pacific. Arguably, the biggest impact of the state independent WWB parameterization was in the number of ENSO events (both warm and cold phases), which appear to be reduced by the inclusion of state independent stochastic forcing. One possibility for this damping is that such forcing enhances cold-water entrainment into the upper ocean, damping ENSO oscillation with little effects on its period. This is also consistent with dynamical systems theory that adding stochastic forcing to a chaotic system reduces the variability (Siqueira and Kirtman, 2012). One future experiment could be to increase the strength of the stochastic WWBs and observe if ENSO is actually further damped.

CCSM4 is slightly more sensitive to state-independent noise forcing than CCSM3. Whether this difference is due to changes in the physics of ENSO in the model or is related to the reduced resolution remains an open question. The increase in tropical Pacific standard deviation does not translate into increased lag-lead correlation. Correlation at all lags remains consistent with the control case. Such lack of sensitivity due to state-independent WWBs forcing is observed in both CCSM3 and CCSM4 models.

For the state-dependent case independent of model version (i.e. CCSM3 or CCSM4), the simulation had more ENSO events, and the bias toward more cold events than warm events was reduced. Here, the number of years with warm or cold events matched those without ENSO, suggesting that the ocean-atmosphere system in the tropical Pacific shifted from an episodic event regime to more of an oscillatory regime. We also detected an increase in ENSO amplitude.

We also used the temporal coherence of ENSO as a diagnostic of the impact of the WWB parameterization. The lag-lead correlations were performed for SSHA along the equator and at 7N with some SSTA indices in regions of high variance. The correlation dropped off quickly away from the zero-lag for the state-independent case, suggesting a comparatively less temporally coherent ENSO. The state-dependent case showed significantly high correlation at longer lags, arguing for a more oscillatory regime. These characteristics were also detected in CCSM4. We also performed composite analysis of SSTA, SSHA, zonal wind stress, and WWBs. Analyzing the five strongest El Niño events suggested that the oscillatory-behavior increased in the state-dependent case with respect to the control. Coherent oscillations at several months lag were detected as precursors to the strongest warm events. Again, similar sensitivity to the WWB parameterization was also found in CCSM4.

There is a clear eastward migration of SSHA for both models, but not for SSTA. The SSTA correlation is simultaneous and maximum over the Niño3.4 region for all experiments. On the other hand, the SSHA shows some lag over the western Pacific, ~9 months for CCSM3 and ~24 months for CCSM4. It can also be observed from Figs. 14 and 15 (composites) that SSTA are fairly stationary in time. There are hints of both eastward and westward propagation, but not as obvious as for SSHA. Such warm or cold SSTA are the result of warm or cold temperature anomalies traveling eastward at thermocline depth, emerging in the eastern Pacific (where thermocline is shallow) then spreading out throughout the equatorial basin. If instead of SSTA lag-correlation, we perform thermocline depth anomaly lag correlation, then a similar pattern to that from SSHA correlation is obtained. But, since SSTA is just the surface response of temperature anomalies at depths, and as a consequence only resurfaces in the eastern Pacific, no eastward propagation is detected from just simple lag correlation or composite analysis.

While it is clear from these results that the state-dependence in the noise has a profound impact on the variability, it is unclear which specific property of the noise is most important. For example, one could decompose the WWBs by amplitude, temporal, and spatial structure and study each of these components separately. This will allow a more detailed understanding of which characteristics of the noise are most important in terms of their state dependence. Ultimately, this might have some feedback on parameterization development. The issue of ENSO predictability in the presence of the WWB parameterization also requires further study. For instance, intuitively one would argue that adding noise to the system should decrease predictability due to increased irregularity of ENSO. However, the increase in oscillatory character and power in the state-dependent case seems to suggest enhanced

predictability. It is interesting that state-independent noise has little effect on both models. Most of the differences were associated with a slight damping of ENSO in the case of CCSM3 and enhanced variability in CCSM4. This difference is depicted in the standard deviation and lag correlation analysis. Correlation becomes larger at zero lag for CCSM4 compared to its control where the opposite occurs with CCSM3. As the lag increases, the correlation drops and the oscillatory pattern observed in the control case disappears. This is consistent for both models, and is consistent with non-linear dynamical system theory (see Siqueira and Kirtman, 2012) that suggested that variability of an unstable non-linear chaotic system is reduced in the presence of additive noise. The reduction in lag correlation at longer lags for the additive noise case is not a surprising result. More surprising is how each model responds to such forcing, which suggests that CCSM3 behaves more like an unstable non-linear chaotic system than CCSM4.

This, along with very little effect on the tropical Pacific seasonal cycle and the contrast by using state-dependent forcing leads to the following conclusion. Based on the results obtained here we conclude that the fast-varying (stochastic) component of the WWB is of little importance in modulating ENSO and tropical Pacific variability due to its inability in projecting its power into interannual frequencies. The slow component (SST related) or deterministic component is playing the bigger role. This result could have repercussions in ENSO predictability and prediction. That is, a forecasting system may only need to capture the basic statistics of the noise forcing instead of aiming at describing its specific details.

## Acknowledgments

This manuscript is part of a Ph.D dissertation of the first author. The first author would like to express thanks to Prof. Chidong Zhang (RSMAS, University of Miami), Prof. Mohamed Iskandarani (RSMAS, University of Miami), and Prof. Robert Burgman (Florida International University). The authors would also like to thank the reviewers for their constructive critiques and suggestions that improved this manuscript. The authors acknowledge support from NSFATM0754341, OCI10749165 and NOAA NA08OAR4320889.

## References

- Blanke, B., Neelin, J.D., Gutzler, D., 1997. Estimating the effect of stochastic wind stress forcing on ENSO irregularity. *J. Clim.* 10, 1473–1487.
- Chen, S.S., Houze Jr., R.A., Mapes, B.E., 1996. Multiscale variability of deep convection in relation to large-scale circulation in TOGA COARE. *J. Atmos. Sci.* 53, 1380–1409.
- Chen, Y.-Q., Battisti, D.S., Palmer, T.N., Barsugli, J., Sarachik, E.S., 1997. A study of the predictability of tropical Pacific SST in a coupled atmosphere–ocean model using singular vector analysis: the role of the annual cycle and the ENSO cycle. *Mon. Weather Rev.* 125, 831–845.
- Chang, P., Wang, B., Li, T., Ji, Li., 1994. Interactions between the seasonal cycle and the Southern oscillation–frequency entrainment and chaos in an intermediate coupled ocean–atmosphere model. *Geophys. Res. Lett.* 21, 2817–2820.
- Chu, P.-S., 1988. Extratropical forcing and the burst of equatorial westerlies in the western Pacific: a synoptic study. *J. Meteor. Soc. Japan* 66, 549–563.
- Collins, W.D., et al., 2006. The community climate system model version 3 (CCSM3). *J. Clim.* 19, 2122–2143.
- Danabasoglu, G., Marshall, J., 2007. Effects of vertical variations of thickness diffusivity in an ocean general circulation model. *Ocean Model.* 18, 122–141.
- Danabasoglu, G., Bates, S.C., Briegleb, B.P., Jayne, S.R., Jochum, M., Large, W.G., Peacock, S., Yeager, S.G., 2012. The CCSM4 ocean component. *J. Clim.* 25 (5), 1361–1389.
- Deser, C., Capotondi, A., Saravanan, R., Phillips, A., 2006. Tropical Pacific and Atlantic variability in CCSM3. *J. Clim.* 19, 2451–2481.
- DiNezio, P.N., Kirtman, B.P., Clement, A.C., Lee, S.-K., Vecchi, G.A., Wittenberg, A., 2012. Mean Climate Controls on the Simulated Response of ENSO to Increasing Greenhouse Gases. *J. Clim.* 25, 7399–7420, <http://dx.doi.org/10.1175/JCLI-D-11-00494.1>.
- Eckert, C., Latif, M., 1997. Predictability of a stochastically forced hybrid coupled model of El Niño. *J. Clim.* 10, 1488–1504.
- Eisenman, I., Yu, L., Tziperman, E., 2005. Westerly wind bursts: ENSO's tail rather than the dog? *J. Clim.* 18, 5224–5238.
- Fasullo, J., Webster, P., 2000. Atmospheric and surface variations in the tropical western Pacific. *Quart. J. Roy. Meteor. Soc.* 126, 899–924.
- Ferrari, Raffaele, McWilliams, J.C., Canuto, V.M., Dubovikov, M., 2008. Parameterization of eddy fluxes near oceanic boundaries. *J. Clim.* 21, 2770–2789.
- Flügel, M., Chang, P., 1996. Impact of dynamical and stochastic processes on the predictability of ENSO. *Geophys. Res. Lett.* 23, 2089–2092.
- Flügel, M., Chang, P., Penland, C., 2004. The role of stochastic forcing in modulating ENSO predictability. *J. Clim.* 17, 3125–3140.
- Gebbie, G.I., Tziperman, E., 2009. Predictability of SST-modulated westerly wind bursts. *J. Clim.* 22, 3894–3909.
- Hartten, L.M., 1996. Synoptic settings of westerly wind bursts. *J. Geophys. Res.* 101, 16997–17019.

- Hendon, H., Wheeler, M.C., Zhang, C., 2007. Seasonal dependence of the MJO–ENSO relationship. *J. Clim.* 20, 531–543.
- Harrison, D.E., Schopf, P.S., 1984. Kelvin wave induced anomalous advection and the onset of surface warming in El Niño events. *Mon. Weather Rev.* 112, 923–933.
- Harrison, D.E., Vecchi, G.A., 1997. Westerly wind events in the tropical Pacific, 1986–95. *J. Clim.* 10, 3131–3156.
- Jin, F.-F., Neelin, J.D., Ghil, M., 1994. El Niño on the devil's staircase: annual subharmonic steps to chaos. *Science* 264, 70–72.
- Jin, F.-F., Lin, L., Timmermann, A., Zhao, J., 2007. Ensemble-mean dynamics of the ENSO recharge oscillator under state-dependent stochastic forcing. *Geophys. Res. Lett.* 34, L03807, <http://dx.doi.org/10.1029/2006GL027372>.
- Jochum, M., Danabasoglu, G., Holland, M., Kwon, W., 2008. Large ocean viscosity and climate. *J. Geophys. Res.* 113, C06017, <http://dx.doi.org/10.1029/2007JC004515>.
- Jochum, M., 2009. Impact of latitudinal variations in vertical diffusivity on climate simulations. *J. Geophys. Res.* 114, C01010, <http://dx.doi.org/10.1029/2008JC005030>.
- Keen, R.A., 1982. The role of cross-equatorial tropical cyclone pairs in the Southern Oscillation. *Mon. Weather Rev.* 110, 1405–1416.
- Kiladis, G.N., Meehl, G.A., Weickmann, K.M., 1994. Large-scale circulation associated with westerly wind bursts and deep convection over the western equatorial Pacific. *J. Geophys. Res.* 99, 18527–18544.
- Kirtman, B.P., 1997. Oceanic Rossby wave dynamics and the ENSO period in a coupled model. *J. Clim.* 10, 1690–1704.
- Kirtman, B.P., Straus, D.M., Min, D., Schneider, E.K., Siqueira, L., 2009. Toward linking weather and climate in the interactive ensemble NCAR climate model. *Geophys. Res. Lett.* 36, L13705, <http://dx.doi.org/10.1029/2009GL038389>.
- Kirtman, B.P., Schopf, P.S., 1998. Decadal variability in ENSO predictability and prediction. *J. Clim.* 11, 2804–2822.
- Kirtman, B.P., Shukla, J., 2002. Interactive coupled ensemble: a new coupling strategy for GCMs. *Geophys. Res. Lett.* 29, 1029–1032.
- Kirtman, B.P., Min, D., 2009. Multimodel ensemble ENSO prediction with CCSM and CFS. *Mon. Weather Rev.* 137, 2908–2930.
- Kirtman, B.P., Fan, Y., Schneider, E.K., 2002. The COLA global coupled and anomaly coupled ocean–atmosphere GCM. *J. Clim.* 15, 2301–2320.
- Kirtman, B.P., Pegion, K., Kinter, S., 2005. Internal atmospheric dynamics and climate variability. *J. Atmos. Sci.* 62, 2220–2233.
- Kleeman, R., 2008. Sensitivity of hybrid ENSO models to unresolved atmospheric variability. *J. Clim.* 21, 3704–3721.
- Kleeman, R., Moore, A.M., 1997. A theory for the limitation of ENSO predictability due to stochastic atmospheric transients. *J. Atmos. Sci.* 54, 753–767.
- Kleeman, R., Tang, Y., Moore, A.M., 2003. The calculation of climatically relevant singular vectors in the presence of weather noise. *J. Atmos. Sci.* 60, 2856–2868.
- Kug, J.-S., Jin, F.F., Sooraj, K.P., Kang, I.-S., 2008. State-dependent atmospheric noise associated with ENSO. *Geophys. Res. Lett.* 35, L05701, <http://dx.doi.org/10.1029/2007GL032017>.
- Kug, J.-S., Sooraj, K.-P., Li, T., Jin, F.-F., 2009. Precursors of the El Niño/La Niña onset and their interrelationship. *J. Geophys. Res.* 115, D5.
- Latif, M., et al., 2001. ENSIP: intercomparison project. *Clim. Dyn.* 18, 255–276.
- Lengaigne, M., Boulanger, J.-P., Menkes, C., Masson, S., Madec, G., Delecluse, P., 2002. Ocean response to the March 1997 westerly wind event. *J. Geophys. Res.* 107, 8015, <http://dx.doi.org/10.1029/2001JC000841>.
- Love, G., 1985. Cross-equatorial influence of winter hemisphere subtropical cold surges. *Mon. Weather Rev.* 113, 1487–1498.
- Luther, D.S., Harrison, D.E., Knox, R.A., 1983. Zonal winds in the central equatorial Pacific and El Niño. *Science* 222, 327–330.
- McPhaden, M.J., 1999. Climate oscillations: Genesis and evolution of the 1997–98 El Niño. *Science* 283, 950–954.
- McPhaden, M.J., 2004. Evolution of the 2002/03 El Niño. *Bull. Am. Meteor. Soc.* 85, 677–694.
- McPhaden, M.J., Freitag, H.P., Hayes, S.P., Taft, B.A., Chen, Z., Wyrki, K., 1988. The response of the equatorial Pacific Ocean to a westerly wind burst in May 1986. *J. Geophys. Res.* 93, 10589–10603.
- McPhaden, M.J., Bahr, F., Du Penhoat, Y., Firing, E., Hayes, S.P., Niiler, P.P., Richardson, P.L., Toole, J.M., 1992. The response of the western equatorial Pacific Ocean to westerly wind bursts during November 1989 to January 1990. *J. Geophys. Res.* 97, 14289–14303.
- McPhaden, M.J., Zhang, M., Hendon, X., H., Wheeler, M., 2006. Large scale dynamics and MJO forcing of ENSO variability. *Geophys. Res. Lett.* 33 (16), <http://dx.doi.org/10.1029/2006GL026786>, issn: 0094–82766.
- Mechoso, C.R., et al., 1995. The seasonal cycle over the tropical Pacific in general circulation models. *Mon. Weather Rev.* 123, 2825–2838.
- Moore, A.M., Kleeman, R., 1996. The dynamics of error growth and predictability in a coupled model of ENSO. *Quart. J. Roy. Meteor. Soc.* 122, 1405–1446.
- Moore, A.M., Kleeman, R., 1999a. The nonnormal nature of El Niño and intraseasonal variability. *J. Clim.* 12, 2965–2982.
- Moore, A.M., Kleeman, R., 1999b. Stochastic forcing of ENSO by the intraseasonal oscillation. *J. Clim.* 12, 1199–1220.
- Münnich, M., Cane, M.A., Zebiak, S.E., 1991. A study of self-excited oscillations in a tropical ocean–atmosphere system, part II. Nonlinear cases. *J. Atmos. Sci.* 48, 1238–1248.
- Murakami, T., Sumathipala, W.L., 1989. Westerly bursts during the 1982/83 ENSO. *J. Clim.* 2, 71–85.
- Neale, R.B., Richter, J.H., Jochum, M., 2008. The impact of convection on ENSO: from a delayed oscillator to a series of events. *J. Clim.* 21, 5904–5924.
- Nitta, T., 1989. Development of a twin cyclone and westerly bursts during the initial phase of the 1986–87 El Niño. *J. Meteor. Soc. Japan* 67, 677–681.
- Nitta, T., Motoki, T., 1987. Abrupt enhancement of convective activity and low-level westerly burst during the onset phase of the 1986–87 El Niño. *J. Meteor. Soc. Japan* 65, 497–506.
- Pan, X., Huang, B., Shukla, J., 2010. Sensitivity of the tropical Pacific seasonal cycle and ENSO to changes in mean state induced by surface heat flux adjustment in CCSM3. *Clim. Dyn.*, <http://dx.doi.org/10.1007/s00382-010-0923-930>.
- Penland, C., Matrosova, L., 1994. A balance condition for stochastic numerical models with application to the El Niño–Southern Oscillation. *J. Clim.* 7, 1352–1372.
- Penland, C., Sardeshmukh, P.D., 1995. The optimal growth of tropical sea surface temperature anomalies. *J. Clim.* 8, 1999–2024.

- Roulston, M.S., Neelin, J.D., 2000. The response of an ENSO model to climate noise, weather noise and intraseasonal forcing. *Geophys. Res. Lett.* 27, 3723–3726.
- Seiki, A., Takayabu, Y.N., 2007. Westerly wind bursts and their relationship with intraseasonal variations and ENSO, Part I. *Statistics. Mon. Weather Rev.* 135, 3325–3345.
- Seiki, A., Takayabu, Y.N., Yasuda, T., Sato, N., Takahashi, C., Yoneyama, K., Shiroyaka, R., 2011. Westerly wind bursts and their relationship with ENSO in CMIP3 models. *J. Geophys. Res.* 116, D03303, <http://dx.doi.org/10.1029/2010JD015039>.
- Siqueira, L., Kirtman, B.P., 2012. Predictability of a low-order interactive ensemble. *Nonlin. Processes Geophys.* 19, 273–282, <http://dx.doi.org/10.5194/npg-19-273-2012>.
- Sooraj, K.P., Kim, D., Kug, J.S., Yeh, S.W., Jin, F.-F., Kang, I.S., 2009. Effects of low-frequency zonal wind variation on the high frequency atmospheric variability over the tropics. *J. Clim. Dyn.* 33, 495–507, <http://dx.doi.org/10.1007/s00382-008-0483-486>.
- Thompson, C.J., Battisti, D.S., 2001. A linear stochastic dynamical model of ENSO, Part II. Analysis. *J. Clim.* 14, 445–466.
- Tziperman, E., Stone, L., Cane, M., Jarosh, H., 1994. El Niño chaos: overlapping of resonances between the seasonal cycle and the Pacific ocean–atmosphere oscillator. *Science* 264, 72–74.
- Tziperman, E., Cane, L.M.A., Zebiak, S.E., 1995. Irregularity and locking to the seasonal cycle in an ENSO prediction model as explained by the quasi-periodicity route to chaos. *J. Atmos. Sci.* 52, 293–306.
- Tziperman, E., Yu, L.L., 2007. Quantifying the dependence of westerly wind bursts on the large-scale tropical Pacific SST. *J. Clim.* 20 (12), 2760–2768.
- Vecchi, G.A., Harrison, D.E., 2000. Tropical Pacific sea surface temperature anomalies, El Niño, and equatorial westerly wind events. *J. Clim.* 13, 1814–1830.
- Verbickas, S., 1998. Westerly wind bursts in the tropical Pacific. *Weather* 53, 282–284.
- Wang, C., Weisberg, R.H., Virmani, J.I., 1999. Western Pacific interannual variability associated with the El Niño–Southern Oscillation. *J. Geophys. Res.* 104, 5131–5149.
- Xue, Y., Cane, M.A., Zebiak, S.E., 1997. Predictability of a coupled model of ENSO using singular vector analysis, Part I. Optimal growth in seasonal background and ENSO cycles. *Mon. Weather Rev.* 125, 2043–2056.
- Yu, L., Weller, R.A., Liu, T.W., 2003. Case analysis of a role of ENSO in regulating the generation of westerly wind bursts in the western equatorial Pacific. *J. Geophys. Res.* 108, 3128, <http://dx.doi.org/10.1029/2002JC001498>.
- Yu, L., Rienecker, M.M., 1998. Evidence of an extratropical atmospheric influence during the onset of the 1997–98 El Niño. *Geophys. Res. Lett.* 25, 3537–3540.
- Zavala-Garay, J., Moore, A.M., Perez, C.L., Kleeman, R., 2003. The response of a coupled model of ENSO to observed estimates of stochastic forcing. *J. Clim.* 16, 2827–2842.
- Zavala-Garay, J., Moore, A.M., Kleeman, R., 2004. Influence of stochastic forcing on ENSO prediction. *J. Geophys. Res.* 109, C11007, <http://dx.doi.org/10.1029/2004JC002406>.
- Zavala-Garay, J., Zhang, C., Moore, A.M., Kleeman, R., 2005. The linear response of ENSO to the Madden–Julian Oscillation. *J. Clim.* 18, 2441–2459.
- Zavala-Garay, J., Zhang, C., Moore, A.M., Wittenberg, A.T., Harrison, M.J., Rosati, A., Vialard, J., Kleeman, R., 2008. Sensitivity of hybrid ENSO models to unresolved atmospheric variability. *J. Clim.* 21, 3704–3721.
- Zhang, C., Gottschalck, J., 2002. SST anomalies of ENSO and the Madden–Julian oscillation in the equatorial Pacific. *J. Clim.* 15, 2429–2445.
- Zebiak, S.E., 1989. Oceanic heat content variability and El Niño cycles. *J. Phys. Oceanogr.* 19, 475–486.
- Zebiak, S.E., Cane, M., 1987. A model El Niño–Southern Oscillation. *Mon. Weather Rev.* 115, 2262.